HHS Public Access

Author manuscript

Nat Chem Biol. Author manuscript; available in PMC 2017 July 12.

Published in final edited form as:

Nat Chem Biol. 2017 January ; 13(1): 81–90. doi:10.1038/nchembio.2238.

Oxidized Arachidonic/Adrenic Phosphatidylethanolamines Navigate Cells to Ferroptosis

Valerian E. Kagan[*,1,2,3,4], **Gaowei Mao**[#,1], **Feng Qu**[#,1], **Jose Pedro Friedmann Angeli**[#,5], **Sebastian Doll**[5], **Claudette St Croix**[6], **Haider Hussain Dar**[1], **Bing Liu**[7], **Vladimir A. Tyurin**[1], **Vladimir B. Ritov**[1], **Alexandr A. Kapralov**[1], **Andrew A. Amoscato**[1], **Jianfei Jiang**[1], **Tamil Anthonymuthu**[1], **Dariush Mohammadyani**[1], **Qin Yang**[1], **Bettina Proneth**[5], **Judith Klein-Seetharaman**[1], **Simon Watkins**[6], **Ivet Bahar**[7], **Joel Greenberger**[4], **Rama K. Mallampalli**[8], **Brent R. Stockwell**[10], **Yulia Y. Tyurina**[1], **Marcus Conrad**[*,5], and **Hülya Bayır**[*,1,9]

[1]Department of Environmental and Occupational Health, University of Pittsburgh, Germany

[2]Department of Pharmacology and Chemical Biology, University of Pittsburgh, Germany

[3]Department of Chemistry, University of Pittsburgh, Germany

[4]Department of Radiation Oncology, University of Pittsburgh, Germany

[5]Department of Helmholtz Zentrum München, Institute of Developmental Genetics, Germany

[6]Department of Cell Biology, University of Pittsburgh, New York

[7]Department of Computational and Systems Biology, University of Pittsburgh, New York

[8]Department of Medicine, University of Pittsburgh, New York

[9]Department of Critical Care Medicine, University of Pittsburgh, New York

[10]Department of Biological Sciences and Chemistry, Columbia University, New York

Abstract

Enigmatic lipid peroxidation products have been claimed as the proximate executioners of ferroptosis - a specialized death program triggered by insufficiency of glutathione peroxidase 4 (GPX4). Here, by using quantitative redox lipidomics, reverse genetics, bioinformatics and systems biology we discovered that execution of ferroptosis involves a highly organized oxygenation center, whereby only one class of phospholipids, phosphatidylethanolamines (PE), undergoes oxidation in the ER-associated compartments with the specificity towards two fatty acyls – arachidonoyl (AA) and adrenoyl (AdA). Suppression of AA or AdA esterification into PE

[*]Correspondence to: Valerian E. Kagan (Kagan@pitt.edu), Marcus Conrad (marcus.conrad@helmholtz-muenchen.de), Hülya Bayır (bayihx@ccm.upmc.edu).

[#]equal contribution

Author contributions

V.E.K., M.C. and H.B. formulated the idea, designed the study and wrote the manuscript. G.M. and J.P.F. performed cell experiments. Y.Y.T. and F.Q. performed MS lipid analysis, interpreted data. C.M.S. and S.W. performed cell imaging experiments. T.A., V.A.T. and A.A.A. performed model systems experiments. D.M. and J.K. performed computational modeling. B.L. and I.B. performed network analysis. S.D., H.D., J.J., V.B.R., A.A.K., B.P. and Q.Y. participated in cell or animal experiments. J.G., R.M. and B.R.S. participated in formulating the idea and writing the manuscript. All authors discussed the results and commented on the manuscript.

Competing financial interests

The authors declare no competing financial interests.

by genetic or pharmacological inhibition of acyl-CoA synthase 4 acts as a specific anti-ferroptotic rescue pathway. Lipoxygenases (LOX) generate doubly- and triply-oxygenated (15-hydroperoxy)-di-acylated PE species which act as death signals while tocopherols and tocotrienols suppress LOX and protect against ferroptosis suggesting an unforeseen homeostatic physiological role of vitamin E. This oxidative PE death pathway may also represent a target for drug discovery.

Keywords

ferroptosis; phosphatidylethanolamine peroxidation; acyl-CoA synthase 4; glutathione peroxidase 4; 15-lipoxygenase; tocopherols and tocotrienols

Introduction

Multicellular eukaryotes have perfected death programs to optimize tissue homeostasis, immune and stress responses and embryogenesis[1]. Such programs are also beneficial for unicellular eukaryotes and - through quorum sensing - for bacteria thus making cell death paradoxically essential for all life kingdoms. On a global scale, redox ferro-ferric cycling of iron by microorganisms controls the planetary fate of this element in the environment[2]. In eukaryotic cells, the same electron donor-acceptor propensities of iron that define its vital role in normal physiology facilitate the ferroptotic death program[3,4].

Ferroptosis is switched-on by the dysregulation of one of the two major redox systems: thiols and lipid peroxidation whereby a combination of glutathione peroxidase 4 (GPX4)/GSH deficiency and activation of one or more putative iron-containing enzymes generate oxygenated lipids as the proximal signals of death[5]. However, neither direct evidence for lipid peroxidation, nor the nature of the oxygenated lipid species responsible for the ferroptotic cell demise has been established. Here, we established that lipoxygenases (LOX), among other iron-containing sources of oxidation, can directly oxidize AA- and adrenoyl(AdA)-phosphatidylethanolamines (PE) into ferroptotic signals facilitated by ACSL4-driven esterification of AA and AdA into PE.

Results

Lipid hydroperoxides accumulate in ferroptotic ER

To induce GPX4 deficiency in mouse embryonic fibroblasts (Pfa1) cells, we used a potent and selective GPX4 inhibitor, RSL3[6]. RSL3 triggered ferroptotic death (Supplementary Results, Supplementary Fig. 1a) and caused a marked decrease in activity of GPX4 (Supplementary Fig. 1b). After chemical inactivation by RSL3, we observed a marked decrease of the protein abundance (Supplementary Fig. 1c) suggesting that GPX4 activity is needed to prevent its instability or degradation.

GPX4 catalyzes the reduction of phospholipid/neutral lipid hydroperoxides to the respective hydroxy-derivatives[7] we endeavored to detect the formation of lipid hydroperoxides in GPX4-deficient Pfa1 cells. We employed live cell imaging with LiperFluo which, similar to GPX4, reduces lipid hydroperoxides to their hydroxy-homologues to yield a fluorescent product[8]. We observed a robust and time-dependent fluorescent LiperFluo response (Fig. 1a,

b) that preceded RSL3 triggered ferroptotic death of WT Pfa1 cells (Fig. 1c). Accumulation of LiperFluo-reactive lipid hydroperoxides occurred extra-mitochondrially (Fig. 1d, upper panel), predominantly in the endoplasmic reticulum (ER) compartment (Fig. 1d, lower panel).

Measurements of reactive oxygen species (ROS) and pro-oxidant activity towards non-lipidic fluorogenic substrates (e.g., a lipid ROS probe, C11-BODIPY 581/591, or linoleamide alkyne click-conjugated by cyclo-addition reaction with fluorescein azide) have been utilized as surrogate measures for lipid peroxidation[9]. While fluorescence responses from these probes showed overall activation during ferroptosis, they could not reveal the direct production of lipid hydroperoxides. Both C11-BODIPY and LiperFluo can react with peroxyl radicals whereas LiperFluo (but not C11-BODIPY) interacts with (phospho)lipid hydroperoxides[10]. By contrast, LiperFluo fluorescence reliably reports intracellular sites of lipid hydroperoxide accumulation[8].

GPX4 reduces hydroperoxides of polyunsaturated fatty acids (PUFA-OOH) and phospholipids (PL-OOH)[7]. Esterification of PUFA into phospholipids requires acyl-CoA synthase catalyzed formation of PUFA-CoA. Specifically, ACSL4 catalyzes synthesis of long-chain polyunsaturated-CoAs with a preference for AA[11], thus facilitating their esterification into phospholipids[12]. While genetic ablation[13] or inhibition of ACSL4 by Triacsin C were both effective in protecting against RSL3 induced cell death (Fig. 1e) we found more robust LiperFluo fluorescence response from Acsl4 KO cells compared to WT cells (Fig. 1a, b). Because Acsl4 KO cells have decreased levels of polyunsaturated-acyl-CoAs (Fig. 1f), they likely accumulate free PUFA-OOH (rather than esterified PL-OOH) causing elevated LiperFluo fluorescence emission. To test this, we performed LC-MS/MS analysis of free PUFA-OOH and PL-OOH in WT *vs* Acsl4 KO cells. This was achieved by the use of platelet-activating factor acetylhydrolase (PAF-AH), an enzyme specifically cleaving the oxidized PUFA residues from phospholipids[14] to yield FA-OOH and lyso-phospholipids. Indeed, in Acsl4 KO cells, RSL3 induced predominantly accumulation of free oxygenated PUFA (Fig. 1g) - in contrast to higher levels of esterified oxygenated AA and adrenic acid (AdA, C22:4) in WT cells (Fig. 1g). Assessments of the reaction rate constants for AA-OOH and purified PE-OOH with LiperFluo in ethanol showed that its reactivity towards free PUFA-OOH was slightly higher than with PL-OOH with the reaction rate constants of $1.6\pm0.1\times10^3 M^{-1}s^{-1}$ [15] and $1.2\pm0.1\times10^3 M^{-1}s^{-1}$, respectively. Thus higher contents of free PUFA-OOH and their higher reactivity toward LiperFluo both contributed to the robust fluorescence response to LiperFluo in Ascl4 KO cells.

AA enhances ferroptotic response in RSL3-treated cells

Suggesting that esterified oxygenated PUFA, act as the proximate executioners of ferroptotic death, we supplemented WT and Acsl4 KO cells with exogenous AA. This resulted in a 24% increase of ferroptosis in RSL3-treated WT cells and only a 13% increase of death in Acsl4 KO cells (Fig. 2a). Accordingly, LC-MS/MS analysis (after PAF-AH treatment) demonstrated higher accumulation of esterified oxygenated AA in phospholipids of WT vs Acsl4 KO cells following RSL3 treatment (Fig. 1g). Additionally, we observed that supplementation with AA triggered elongation activity resulting in the increased content of

AdA and its oxygenated forms (Fig. 2b, c). The amounts of oxygenated esterified AA and AdA were lower in RSL3-treated Acsl4 KO cells than in RSL3-treated WT cells (72.2±27.0 and 28.2±8.0 compared to 199.3±26.2 and 137.8±77.7 pmol/μmol phospholipids, respectively, $p<0.01$) (Fig. 2d).

Remodeling of phospholipids via the Land's cycle re-acylation requires insertion of an acyl group into lyso-phospholipid, an enzymatic step catalyzed by lyso-phosphatidylcholine acyltransferase 3 (LPCAT3), specific towards long-chain phosphatidylcholine (PC)- and PE-based substrates. Accordingly, knockdown of Lpcat3 caused increased resistance of mouse lung epithelial (MLE) (Fig. 2e) and mouse embryonic cells (Supplementary Fig. 1d) to ferroptosis triggered by RSL3, in line with a previous report[16].

Redox phospholipidomics of ferroptotic signals

Among the eight distinct isoforms of GSH peroxidases, only GPX4 can reduce PL-OOH in membranes. To identify the pro-ferroptotic oxygenated phospholipids we performed global redox phospholipidomics LC-MS/MS analysis of RSL3-treated WT and Acsl4 KO Pfa1 cells, as well as Gpx4 KO Pfa1 cells and kidney cells from Gpx4 KO mice. Overall, we detected 350 individual species of phospholipids in five major classes – PC, PE, phosphatidylserine (PS), phosphatidylglycerol (PG), phosphatidylinositol (PI) and cardiolipin (CL) – in Pfa1 cells (Fig. 3a). This included 220 non-oxygenated and 130 oxygenated phospholipid species, respectively. Oxygenated derivatives with different numbers of oxygen atoms were found in all these major classes of phospholipids with the notable exception of CL (Fig. 3b and Supplementary Fig. 2a). Most oxygenated phospholipids displayed a trend towards their increased contents in ferroptotic cells with the differences between them being both fold-increase and the significance of the changes. Therefore, we utilized these two features to rank them as the most likely lipid death signals (Fig. 3b, c). We applied a series of quantitative inclusion criteria (Supplementary Fig. 3): 1) significantly increased content (≥3-fold) in ferroptotic *vs* control cells, $p<0.05$); 2) correlation with cell death with R>0.7; 3) reduced contents of non-oxygenated oxidizable precursors in Acsl4 KO cells 4) elevated levels in Gpx4 KO cells *in vitro* and Gpx4 KO mice *in vivo* (see below). Application of these criteria sequentially reduced the number of candidates from 110 to 44 (after criterion 1), to 17 (after criterion 2, R values are shown in Supplementary Table 1), to 8 (after criterion 3), to 4 (after criterion 4) (Fig. 3d and Supplementary Fig. 2b, c). Only four molecular species of phospholipids in only one class of phospholipids – doubly- and triply-oxygenated species of PE passed the scrutiny of the sieving criteria.

Oxygenated PE in Gpx4 KO cells and kidney

In a model of genetic depletion of GPX4, we also observed that death in Gpx4 KO cells (Supplementary Fig. 4)[17] was accompanied by elevated contents of doubly- and triply-oxygenated AA- and AdA-containing PE species (Fig. 4a, b, c). We previously found that depletion of GPX4 *in vivo* caused acute renal failure, accumulation of oxygenated phospholipids and ferroptosis[18]. LC-MS analysis revealed accumulation of 10 oxygenated PLs in kidney of tamoxifen-inducible Gpx4 KO mice 8 days after knockout induction. Notably, the same di- and tri-oxygenated PE species (C18:0/C20:4 and C18:0/C22:4) were

found as in Gpx4 KO cells or RSL3 treated cells *in vitro* (Fig. 4d, e and Fig. 5a, b, respectively). Their elevated levels were attenuated in mice treated with a ferroptosis inhibitor, Liproxstatin-1 (Fig. 4f).

The Venn diagram (Supplementary Fig. 5a) illustrates the commonality of four oxygenated PE species in the four different ferroptotic conditions, including RSL3 in WT and Acsl4 KO, Gpx4 KO (*in vitro*) and Gpx4 KO (*in vivo*). The specificity of death signals is emphasized by the following two facts: i) out of 62 total PE species and 36 oxidizable PUFA-containing PE species, only 2 were identified as precursors of ferroptotic signals (Supplementary Fig. 5b); (ii) out of 57 oxygenated PEs, only 4 were identified as specific ferroptotic signals (Supplementary Fig. 5c).

To further validate the identified oxygenated PE species as lipid death signals, we applied multivariate data analysis. Clear stratification of the data indicated the existence of potential biomarkers thus permitting to narrow down the phospholipid oxidation products with R2Y(cum)=0.953, Q2(cum)=0.908 (Supplementary Fig. 5d). All four oxygenated PEs were confirmed as biomarkers with variable importance values for the projection (by OPLS-DA) greater than 1 (Supplementary Fig. 5e).

LC-MS/MS identification of ferroptotic signals

By employing stable isotopic labeling with *d8*-AA, we established that *d8*-AA can be elongated into *d8*-AdA that was detectable as free fatty acid along with *d8*-AA-CoA, *d8*-AdA-CoA (Supplementary Fig. 6) and a variety of relatively abundant *d8*-AA-containing and *d8*-AdA-containing phospholipids (Fig. 5c). Significant accumulation of di- and tri-oxygenated di-acyl-PE species containing C18:0/d8-C20:4 and C18:0/d8-C22:4 in *sn-2* position was detected in RSL3-triggered cells (Fig. 5a, b). No changes in the content of alkyl- or alkenyl-PE species were found (Fig. 5d). Accumulation of non-deuterated and deuterated PE was more robust in WT cells than in Ascl4 KO cells (Fig. 5c and Supplementary Fig.7).

Addition of RSL3 to *d8*-AA supplemented cells resulted in the formation of 20 deuterated oxygenated phospholipid species (110 of the total 130 remained non-deuterated). Among them, accumulation of mono-, di- and tri-oxygenated species of di-acyl-PE was revealed (Fig. 5a, b). MS/MS analysis confirmed the presence of oxidatively modified AA (Fig. 5e) and AdA (Supplementary Fig. 8a) in PE. These species were similar to those formed in non-supplemented cells (Fig. 5a, b) and their content was lower in Acsl4 KO cells *vs* WT cells. Tri-oxygenated deuterated PE products were not detectable in cells lacking ACSL4 (Fig. 5a, b). Only small accumulation of *d8*-AA was detected in PC which was not affected by Acsl4 KO (Supplementary Fig. 8b). Thus oxidation of AA- and AdA-containing PE represents the major pathway for ferroptotic signaling.

PE ferroptotic precursors are decreased in Acs4 KO cells

AA/AdA esterification into PE can be pharmacologically suppressed by rosiglitazone.[13,19] Lipidomics of Pfa1 wt cells and Acsl4 KO cells treated with rosiglitazone (30μM, for 72 h) revealed reduced level of PE molecular species with C18 fatty acids (C18:0 or C18:1) at *sn-1* position and C20:4 or C22:4 fatty acids at *sn-2* position - oxidation substrates for

ferroptotic signals (Supplementary Fig. 9a). This effect was similar in Acsl4 KO cells - decreased contents of the same PE species (Supplementary Fig. 9b). Rosiglitazone did not cause these changes in Acsl4 KO cells[1319]. The rosiglitazone effects were specific to C18 PE species at *sn-1* position as no differences in the contents of PE with C16 fatty acids at *sn-1 position* – which are not oxidized to pro-ferroptotic death signals - were observed (Supplementary Fig. 9). Principal component analysis showed that rosiglitazone and ACSL4 deficiency caused similar changes in PE profiles[13]. Clustering analysis demonstrated that PE profiles in WT cells exposed to rosiglitazone were similar to those found in both non-treated and treated Ascl4 KO cells.

Direct oxygenation of PE generates ferroptotic signals

There are two alternative pathways for PE oxygenation during ferroptosis: i) non-oxygenated AA/AdA (or their acyl-CoA-forms) are esterified into PE followed by PE oxygenation, or ii) oxygenation of free AA/AdA (or their acyl-CoA-forms) with the subsequent esterification into PE. Accordingly, resistance of Acsl4 KO cells to ferroptosis induction may be due to either lower levels of AA-PE and AdA-PE undergoing subsequent oxygenation or to lower integration of oxygenated AA or AdA into PE. We found that 15-LOX readily oxidizes AA-CoA yielding AA-OOH-CoA with characteristic LC-MS fragmentation profiles (Supplementary Fig. 10). However, biosynthetically pre-formed AA-OOH-CoAs failed to stimulate RSL3 induced ferroptosis (beyond the stimulatory effect of AA or AA-OOH) in either WT or Acsl4 KO cells (Fig. 6a). Moreover, no oxygenated AA-CoA or AdA-CoA – AA-OOH-CoA and/or AdA-OOH-CoA – were detected in either WT or Acsl4 KO cells challenged with RSL3. Further, oxygenated AA-PE and AdA-PE accumulated during RSL3-triggered ferroptosis in WT cells (Fig. 5a, b). Finally, exogenously pre-formed PE-AA-OOH (Fig. 6b) – but not AA-OOH (Fig. 6a) – strongly enhanced RSL3 triggered ferroptosis in Acsl4 KO cells thus directly demonstrating the role of PE-OOH as a ferroptotic death signal overriding the insufficiency of AA esterification into PE. After supplementation, the PE-OOH content in cells was ~6 nmol/μmol phospholipids, i.e. comparable with that in AA-treated WT cells exposed to RSL3.

To authenticate the oxygenated PE species, we oxidized PE-(C18:0/C20:4) by human 15-LOX in the presence of lysates from control and GPX4 deficient (RSL3 treated, 6 hrs) cells and established by LC-MS/MS (Supplementary Fig. 11a) that the enzymatic products were identical to the PE species with singly-, doubly- and triply-oxygenated AA detected in ferroptotic cells (Fig. 5e). In the presence of RSL3 treated cell lysates, higher levels (*vs* control cells) of doubly oxygenated hydroperoxy-PE species (PE-OOH) were found (Supplementary Fig. 12). Further, we purified PE-OOH (prepared by pre-oxidation of PE-(C18:0/C20:4) by 15-LOX), incubated the purified product with cell lysates and performed MS/MS analysis. We confirmed the structure of singly- and doubly-oxygenated PE as 15-hydroxy-AA-PE (Supplementary Fig. 11c) and 15-hydroperoxy-AA-PE species (Fig. 6c). The MS^2 and MS^3 analysis revealed that tri-oxygenated PE species were represented by 15-hydroperoxy-8-hydroxy-AA-PE, 15-hydroperoxy-9-hydroxy-AA-PE and 15-hydroperoxy-12-hydroxy-AA-PE (Fig. 6c). Moreover, we observed that 15-LOX added to cell lysates from RSL3 treated cells generated more PE (C18:0/C20:4+3[O]) and less PE

(C18:0/C20:4+1[O]) than WT cells (Supplementary Fig. 12). Similar results were obtained using Gpx4 KO cell lysates (Supplementary Fig. 11b).

Enzymatic generators of peroxidation signals

Several enzymes – LOX, cyclooxygenases (COX) and cytochrome P450 (CYP450) – can oxygenate AA and AdA. Among several specific regulators, inhibitors of LOX but not COX or CYP450 were effective in preventing ferroptotic death (Fig. 6d). Accordingly, liproxstatin inhibited the 15-LOX enzymatic activity (Supplementary Fig. 13) and suppressed the production of pro-ferroptotic oxygenated PE *in vivo* (Fig. 4f). Computational modeling showed that liproxstatin-1 binds with 15-LOX with high affinity (binding energy −8.1 ± 0.2 kcal/mol). In contrast, COX cannot effectively utilize esterified PUFA as the substrate[20]. Some isoforms of CYP450 (e.g., P450 2W1) oxidize free FA at low rates and catalyze oxidation (epoxidation, hydroxylation) of *sn-1* PUFA lyso-phospholipids 21. Notably, di-acyl-glycerophospholipids are not utilized by CYP450 as oxygenation substrates. We further established that etomoxir, an inhibitor of PUFA β-oxidation, did not suppress but rather stimulated RSL3-induced cell death (Fig. 6e). This suggests that preservation of PUFA for enzymatic oxygenation reactions was conducive of the production of cell death signals.

Vitamin E regulates ferroptosis via LOX suppression

Vitamin E family comprises several homologues of tocopherols and tocotrienols known to effectively inhibit LOXes[22]. Both tocopherols and tocotrienols protected against ferroptotic death in Gpx4 KO cells (Supplementary Fig. 14a) whereby the effectiveness of tocotrienols was overall markedly higher than that of tocopherols – in line with their higher effectiveness to inhibit LOX PUFA oxygenation. While tocopherols strongly suppress non-regio-specific free radical component of LOX-catalyzed peroxidation of phospholipids[23], they can also act via competition for the PUFA substrates binding sites (ie, via the “corking” mechanism). Computational modeling showed binding of LOX with different members of vitamin E family with a higher affinity for tocotrienols vs tocopherols (Supplementary Fig.14b). If the competitive binding of tocopherols contributes to the suppression of LOX activity, then esterified derivatives of tocopherols should also exert this effect in spite of the lack of radical scavenging chromanol hydroxy-group. Using ESR spectroscopy, we confirmed that 15-LOX was ineffective in generating tocopheroxyl radicals, one-electron oxidation intermediates from α-tocopherol succinate (TS) or α-tocopherol phosphate (TP) which were readily detectable as partially resolved characteristic signals from either α-tocopherol or α-tocotrienol (Supplementary Fig. 14c). However, both esterified analogs acted as 15-LOX inhibitors whereby TS was markedly more efficient that TP (Supplementary Fig. 14d). Suppression of 15-LOX activity by TS was quantitatively comparable to that of α-tocotrienol. Further we performed LC-MS assessments of changes in the contents of α-tocopherol, TP, TS and α-tocotrienol after incubation with 15-LOX and AA. The levels of TS and TP were only slightly affected by the enzyme (Supplementary Fig. 14e). Thus, radical scavenging can contribute to the inhibitory effects of α-tocopherol and α-tocotrienol along with their ability to compete for the substrate binding site (Supplementary Fig. 14). For TS and TP, the “corking” mechanism may be the major contributor to the inhibition of the activity. Accordingly, computational modeling demonstrated that TS and TP interacted with the protein via the tail-in orientation (Supplementary Fig. 14b).

LOX oxidizes non-bilayer phospholipid arrangements

Phospholipase A2 (PLA2) phospholipid hydrolysis controls the availability of free PUFA to initiate the conventional LOX biosynthesis of lipid mediators[24]. How is AA esterified into abundant phospholipids recognized by LOX? Our computational modeling demonstrated feasibility of oxygenation of AA esterified into PE by 15-LOX: the binding energies were similar for free and esterified PUFA (Supplementary Fig. 15a). The question remains how the enzyme chooses its substrates from numerous AA-containing phospholipids. One possible mechanism may be preferential attack of non-bilayer arrangements of phospholipid substrates providing an easier access for the LOX. Notably, PE typically forms non-bilayer arrangements in the membrane[25]. To test this, we used stearoyl-AA-PE (SAPE) that forms non-bilayer (hexagonal) phases[26] and compared its oxidation with stearoyl-AA-PC (SAPC) with the typical bilayer organization (Supplementary Fig. 15b). SAPE was a much better 15-LOX substrate than SAPC (Supplementary Fig. 15b). AA-OOH-PE species were detected as the major oxidation products. These results are supported by our coarse-grained molecular dynamics simulations demonstrating a robust binding of 15-LOX with SAPE *vs* essentially no binding with SAPC (Supplementary Fig. 15c and Supplementary Table 2).

Modeling of ferroptotic phospholipid metabolic network

We further constructed a mathematical model (47 differential equations) for the production of oxygenated PE species based on a simplified network of main metabolic reactions regulating ferroptosis and focused on the GPX4/AA(AdA)-PE-driven ferroptotic responses (Supplementary Fig. 16a, Supplementary Tables 3–5). The model quantitatively reproduced not only the dataset for the model calibration (Supplementary Fig. 16b–e), but also the additional dataset reserved for model validation (Supplementary Fig. 16f–g). This indicates that the network covers key ferroptotic regulators and, possibly the effects of other mechanisms that are not included in the model but are implicitly captured by the model parameters (Supplementary Figs. 16h–j and 17a, b).

Discussion

Ferroptosis is a newly coined term for one of the programmed death pathways associated with the dysregulation of thiol and lipid oxidative metabolism controlled by GPX4. GPX4 deficiency leads to the accumulation of reactive lipid electrophiles[27]. Given the unique ability of GPX4 to catalyze the reduction of PL-OOH, their accumulation of is highly likely in the context of GPX4 deficiency. In spite of the commonly suggested role of phospholipid peroxidation products in ferroptosis, identification of the proximate phospholipid peroxidation products has not been accomplished. This work identified four individual molecular species of doubly- and triply-oxygenated di-acyl AA/AdA-containing species of PE containing 15-hydroperoxy-groups as ferroptotic death signals. Oxygenation attack occurs on AA/AdA-PE but not via re-esterification of pre-oxidized free fatty acids into phospholipids. Exogenous AA/AdA-PE-OOH – but not free AA-OOH or AdA-OOH - caused ferroptotic cell death. Mono-oxygenated PE products - formed by esterification of enzymatically pre-synthesized free eicosanoids - have been implicated in signaling functions of innate immune cells[20]. These products, however, were formed by fast esterification of enzymatically pre-synthesized free eicosanoids and the relevant reactions were localized

predominantly to the nuclear and extranuclear membrane. Direct oxygenation of PUFA-PE species by 12/15-LOX has been documented in plasma membranes of resident macrophages as a required mechanism for the uptake and phagocytosis of apoptotic cells[28].

Oxidation of CLs – a required step in the execution of apoptosis[29] - was not involved in ferroptotic signaling. Thus redox signaling in apoptosis and ferroptosis is based on specific engagement of two different classes of phospholipids – CL and PE with different acyl molecular speciation - linoleic acid (C18:2) oxygenation in CLs and AA/AdA oxygenations of PE. The oxygenating enzymes are also different – cytochrome c[30] and likely 15-LOX, respectively. Live cell imaging demonstrated predominant accumulation of PE-OOH in the extra-mitochondrial ER-associated compartments where several iron proteins – COX, LOX and CYP450 – can generate PUFA lipid hydroperoxides[31]. Of those, only LOXes, however, utilize di-acyl lipids as their substrates[32] thus making these non-heme-iron enzymes possible candidate-catalysts of ferroptotic oxygenated PE-species. Our model biochemical experiments and computer simulations indicate that a non-bilayer (possibly hexagonal) arrangements of Aa/AdA-PE – in contrast to highly ordered bilayer organization of AA-PC - facilitates the availability of these PL substrates for binding and the enzymatic attack by 15-LOX. It is also possible that the prevalence of PE in the inner leaflet of plasma membrane[33,34] contributes to the preferential oxidation by LOX, whereas confinement of PC to the outer membrane monolayer is not conducive of its interactions with the intracellular oxidizing machinery.

A highly organized oxygenation center in the ER-associated compartment may be functionally involved in the production of eicosanoids and docosanoids under redox control of GPX4 over metabolic reaction of PUFA-OOH. Insufficiency of this control caused by genetic or chemical inactivators leads to the accumulation of excessive amounts of highly electrophilic and diffusible lipid mediators threatening the existence of many surrounding cells. Insufficiency of GPX4 triggers lipid metabolic pathways for the enhanced production of AA/AdA-containing di-acylated PEs as substrates of LOX catalyzed reactions. This leads to the generation of doubly- and triply-oxygenated 15-hydroperoxy-containing PE species acting as lipid death signals. The significance of functional association of ACSL4, Elongase 5, LPCAT3 and LOX – for the production of PE-AA-OOH and PE-AdA-OOH is further emphasized by the systems biology analysis which confirmed high sensitivity of several key-enzymes - ACSL4, LPCAT3 and 15-LOX - for ferroptosis. Notably, the presence of LOXes has been discovered in prokaryotes, Pseudomonas aeruginosa, lacking polyunsaturated lipid substrates[35]. It appears that the bacteria utilize secretable LOX to cause “ferroptotic death” of target epithelial cells. This suggests that LOX-driven selective oxidation of esterified PE may represent a highly conserved and ancient mechanism of cell death.

The essentiality of esterified oxygenated PUFA explains the recently demonstrated importance of ACSL4 and LPCAT3 as participants of ferroptotic lipid signaling thus offering new pharmacological targets for drug discovery[13,16]. Moreover, different forms of vitamin E, particularly tocotrienols, are effective in protecting against ferroptotic death. Thus one of the physiologically possible mechanisms of vitamin E action may be specific liganding of the LOX catalytic site outcompeting binding and oxygenation of free or PE-esterified AA and AdA. Our computational modeling of free PUFA, including AA and AdA,

clearly shows that the tail-in orientation is the dominant alignment of the substrate in the catalytic site. Previous studies using a Quantum Mechanics/Molecular Mechanics approach[36] have shown that hydrogen abstraction from C13 by 15-LOX-2 is only consistent with the "tail-in" orientation of AA, while its carboxylate group interacts with Arg429 located at the opening of the substrate binding site.

It has been reported that 15-LOX generates not only regio-specific (phospho)lipid hydroperoxides but also random hydroperoxides as side reaction products[37]. Radical-scavenging antioxidants (α-tocopherol, 2-carboxy-2,5,7,8-tetramethyl-6-chromanol), were more effective towards inhibiting the formation of random oxidation products rather than regio-specific products. Thus not only free radical scavenging but also competition with the oxidation substrates for the binding site of the protein ("corking" mechanism) may be an important factor contributing to the inhibition of stereo-specific LOX-driven oxidations. Several reports documented efficiency of Vitamin E as a protector of cells against ferroptotic death in vitro[38–40]. In previous publication[18], we reported that α-tocopherol was effective in preventing ferroptosis in nM-range of concentrations. More importantly, this protective effect of vitamin E was also realized in vivo[41]. It has been established that "$Gpx4^{-/-}$ pups born from mothers fed a vitamin E-enriched diet survived, yet this protection was reversible as subsequent vitamin E deprivation caused death of GPX4-deficient mice ~4 weeks thereafter"[38]. Thus vitamin E can be considered as an effective anti-ferroptotic agent. Our data show that tocotrienols are even more effective in protecting cells against ferroptosis. This higher efficiency may be due not only to a known better integration of tocotrienols into cells[42], but also to their more effective competing with the PUFA-PL substrates for the binding sites on 15LOX. As 15-LOX is an important contributor to pro-ferroptotic PE-peroxidation, significant inhibitory activity of TP and TS towards 15-LOX – in the absence of radical scavenging hydroxy-groups – points to an alternative mechanism of their action such as competition for the substrate binding site (i.e., "corking").

It has been proposed to utilize the enhanced ferroptotic death pathway to eradicate cancer cells resistant to pro-apoptotic stimulation[43]. Given the stimulatory role of AA, AdA, in inducing ferroptotic cell death there may be nutritional approaches to treatment of cancer combined with ferroptotic inducers (e.g., RSL3, or other inducers or GSH depletion) for enhanced anti-cancer therapy. In particular, an antitumor phenolic drug, etoposide, will be effectively removing GSH in myeloperoxidase–rich myelogenous leukemia cells thus incapacitating GPX4 and triggering ferroptosis. It is tempting to speculate that mechanisms of several well characterized regulators of ferroptosis – regulators of GSH synthesis and transport, redox-sensitive Nrf2 signaling pathway, metabolic regulators of iron uptake and metabolism – universally converge on the specific oxygenation of PE as ferroptotic signals.

ONLINE METHODS

Materials

All the lipid standards and 1-stearoyl-2-arachidonoyl phosphatidylethanolamine (SAPE) and 1-stearoyl-2-arachidonoyl phosphatidylcholine (SAPC) were purchased from Avanti Polar Lipids Inc. AquaBluer was obtained from MultiTarget Pharmaceuticals. The Cytotoxicity Detection Kit for measuring the released lactate dehydrogenase (LDH) was purchased from

Promega. LiperFluo was purchased from Dojindo Molecular Technologies, Inc. Deuterated arachidonic acid (d8-AA), Triacsin C, and AA-hydroperoxy-derivative (AA-OOH), pletelet-activating factor-acetylhydrolase (PAF-AH), 15-LOX from Glycinemax, recombinant human 15-LOX-2 were purchased from Cayman Chemical. 5-(Methylamino)-2-(1-naphthalenyl)-4-oxazolecarbonitrile (ML351), 6,11-dihydro-[1]benzothiopyrano[4,3-b]indole (PD146176), 4-Hydroxy-2-methyl-3-(pyrid-2-yl-carbamoyl)-2H-1,2-benzothiazine 1,1-dioxide (Piroxicam), N-(methylsulfonyl)-2-(2-propynyloxy)-benzenehexanamide (MSPPOH), (±)-N-hydroxy-N-(1-benzo[b]thien-2-ylethyl)urea (Zileuton), and N-[(8-Hydroxy-5-nitro-7-quinolinyl)-2-thienylmethyl]-propanamide (NCTT-956) were purchased from Sigma-Aldrich. GPX4 antibody (cat. # ab125066) was purchased from Abcam ß-actin antibody was from Sigma (cat. # A3854), primary Lpcat3 antibody, MBOAT5 (D-19) goat polyclonal IgG (cat. # sc-161831) were from Santa Cruz Biotechnology Inc. Secondary anti-goat IgG (whole molecule)-peroxidase antibody was produced in rabbit (cat. # A5420-1mL) and purchased from Sigma-Aldrich All other reagents were purchased from Sigma-Aldrich unless indicated.

Gpx4 KO mice

In vivo experiments with C57BL/6J female/male mice (8–10 weeks obtained from Charles River Laboratories International, Inc. were performed in Helmholtz Zentrum, Institute of Developmental Genetics (Münich, Germany). Generation of mice with *Gpx4* alleles (Gpx4 flox/flox (Gpx4tm2Marc)) referred to as Gpx4 KO) was performed as previously described[17]. For the pharmacological inhibitor experiments, the $CreER^{T2}$; $Gpx4^{fl/fl}$ mice were injected on days 1 and 3 with 0.5 mg 4-hydroxytamoxifen dissolved in Myglyol. On day 4, compound treatment was started (Liproxstatin-1: 10 mg/kg) along with vehicle control (1% DMSO in PBS). Liproxstatin-1 and vehicle control were administered once daily by i.p. injection. Vehicle is colorless and Liproxstatin - 1 is white to light brown and has indistinguishable odor, ensuring no detectable bias. Supplementation of drinking water was done in a blinded fashion and animal behavior was assessed daily in the treatment experiment. Animals included in the treatment study were randomly distributed between both sexes and weight, with typically 8–10 weeks of age. The average weight between the groups was typically between 22 and 24 g. For the treatment experiments, groups were formed in order to have comparable numbers of females/males of the same age. Weight of the animals was also arranged in order to have a similar distribution between females and males. The injections and collection of (terminal) animals were blinded. When animals showed terminal signs, they were sacrificed according to European animal welfare law. The treatment experiment using the inducible Gpx4−/− mice was approved by the “Regierung von Oberbayern” (Bavaria, Germany) and performed under the animal protocol number 55.2-1-54-2532-144-12. Kidney tissues from mice were obtained from Helmholtz Zentrum, Institute of Developmental Genetics.

Cell lines conditions and treatments

Mouse embryonic fibroblasts (MEF) were purchased from ATCC. Cell line was STR profiled at ATCC. Acsl4 KO cells were generated using CRISPR/Cas9 technology[13]. Cas9-expressing mouse embryonic fibroblasts (Pfa1) were transfected with a plasmid expressing a gRNA targeting exon 1 of the Acsl4 gene. Gpx4 conditional KO cells were generated by

Cre/LoxP technology and described previously[17]. 4-hydroxytamoxifen (Tam) was used to initiate the MERCreMER (MER, mutated-estrogen receptor) mediated excision of the floxed Gpx4 alleles resulting in Gpx4 KO cells. Mouse lung epithelial cells (MLE) cells were purchased from ATCC. MLE were cultured in HITES medium (DMEM:F12, 1:1 mix, with 5 μg/ml Insulin, 10 μg/ml Transferin, 30 nM sodium selenite, 10 nM hydrocortisone, 10 nM β-estradiol, 10 mM Hepes and 2 mM L-glutamine) supplemented with 10% FBS, 100U/ml penicillin and 100 μg/ml streptomycin. All the cells were maintained in Dulbecco's Modified Eagle's Medium (DMEM) with 10% fetal bovine serum (FBS), 100 U/ml penicillin, and 100 μg/ml streptomycin. Cells were grown in incubators with controlled temperature of 37°C, CO2 of 5% and humidity of 95%. All the cell lines used here underwent routine mycoplasm tests in our laboratory and were negative. Treatments: WT and Acsl4 KO cells were pretreated with either arachidonic acid (AA) (2.5 μM), 15-hydroperoxy-AA (AA-OOH) (2.5 μM) or 15-hydroperoxy-arachidonoyl-CoA (AA-OOH-CoA) (2.5 μM) in complete medium for 16 hrs followed by RSL3 treatment. In most experiments, RSL3 treatments were performed using a concentration of 100 nM for 6 hrs. For MLE, RSL3 was used at 0.5 and 1.0 μM concentration for 6 hrs. Cell viability was assessed by propidium iodide staining or LDH release unless stated otherwise.

Treatment with 15-hydroperoxy-AA-phosphatidyletanolamine (PE)

WT and Acsl4 KO cells were treated with RSL3 (100 nM) in complete medium for 2 hrs followed by 1-stearoyl-2-arachidonoyl-PE-OOH (SAPE-OOH, 0.45, 0.6, 0.9 μM) for another 4 hrs in the presence of RSL3 before cell death analysis. Cells were harvested by trypsinization for further analysis.

Live Cell Imaging

Cells were seeded in 35-mm glass-bottomed tissue culture dishes (MatTek Corp.) prior to infection with an adenoviral vector expressing either the mitochondrially targeted (mFAP), or ER targeted (ER-FAP) fluorogen activating protein[44]. At 48 hrs following transfection, cells were pre-stained with 10 μM liperfluo (green) for 30 min before cells were treated with 100 nM RSL3. Before imaging, cells were also loaded with 5 nM malachite green to reveal the mFAP transgene (thereby defining the mitochondria or ER compartments[45]. All images were acquired using a Nikon Ti inverted microscope (Nikon Inc.) equipped with a 60X 1.49NA oil optic, SpectraX diode based light source (Lumencor), Chroma Technology Inc. filer sets, and an ORCA-Flash4.0 V2 digital cMOS camera (Hamamatsu photonic K.K.). Images were acquired and analyzed using NIS-Elements software (Nikon Inc.)

Assessment of GPX4 activity

The activity measurements in cell lysates were performed in 0.1 M Tris –HCl (pH 8.0), containing 0.5 mM EDTA and 1.25% Triton X-100, 0.2 mM NADPH, 3 mM glutathione, glutathione reductase (1 U/ml), 0.5 mg of cell protein. Oxidized tetralinoleoyl cardiolipin (final concentration 50 μM) was used as a substrate. The amount of oxidized GSH was calculated based on the amount of NADPH consumed during GSSG reduction (molar extinction coefficient of NADPH at 340 nm is 6.2×10^3 $mol^{-1}cm^{-1}$).

Western blot analysis of GPX4

Western blotting analysis was used to determine the level of GPX4 in the MEF cells. An equal amount of proteins was loaded in each lane. Proteins were separated by gradient 8–16% Tris-Glycine Gels (Precise™ 8–16% Tris-Glycine Gels, 25ul/well, 15 well) (Life Technologies) and electrically transferred to a polyvinylidene difluoride membrane (Bio-Rad). After blocking the membrane with 5% skim milk, target proteins were immunodetected using GPX 4 antibody at 1:500 (ab125066, Abcam) following overnight incubation at 4°C. Thereafter, the horseradish peroxidase (HRP)-conjugated anti-rabbit IgG H&L at 1: 2000 (ab6721, Abcam) was applied as the secondary antibody, and the positive bands were detected using Amersham ECL plus Western blotting detection reagents (GE Health care).

Lpcat3 Knock-down

For the generation of Lpcat3 KD in MLE or MEF cells, we used pSico plasmid (Addgene plasmid # 11578), a lentivirus based Cre-lox-regulated RNA interference system. Briefly, shRNAoligos (Sense: 5′ TGGCTTAAGGTGTACAGATCTTCAAGAGAGATCTGTACACTTTAAGCCTTTTTTC 3′; antisense: 5′TCGAGAAAAAAGGCTTAAGGTGTACAGATCTCTCTTGAAGATCTGTACACCTTA AGCCA 3′) (Integrated DNA Technologies Inc., Coralville, IA) were annealed by heating the sense and anti-sense oligos in annealing buffer for 4 min at 95°C and then allowing to cool to room temperature. Annealed oligos were ligated to pSico vector at HpaI and XhoI sites (Takara Bio USA, Inc.) with T4-DNA ligase enzyme (Promega). DNA was isolated from the right clone and transfected into MLE/MEF cells using lipofectamine 3000 reagent (Invitrogen). Transfected cells were sorted (3 times) by selecting only GFP positive cells by Flow-cytometry (BD FACSAria II). After the third sorting, more than 90% cells were stable GFP-positive cells. To these cells, TAT-Cre Recombinase (Excellgen) protein (1 μM) was added and after 48, 72, and 96 hrs for MLE or 72 hrs for MEF, the efficiency of LPCAT3 KD was determined by western blotting using anti-LPCAT3 antibody (Sc-161831, Santa Cruz Biotechnology Inc.).

Western blot analysis of LPCAT3

Cells were harvested by trypsinization, washed with PBS, re-suspended in phosphate buffer (pH 7.8) and sonicated on ice. Protein concentrations were determined with Bradford protein assay kit (ThermoFisher Scientific). Equal amounts of protein were separated by 10% SDS-PAGE, electrotransferred by semidry blotting onto a nitrocellulose membrane and probed with primary antibodies against LPCAT3 at 1:1000 dilution. Immunoreactive bands were detected by chemiluminescence kit. The bands were visualized using X-ray film and imaged with computerized digital imaging system. (ImageJ software, NIH). Actin antibody for loading corrections.

Preparation of hydroperoxy PE

1-steraoyl-2-arachidonoyl-PE was oxidized by 15-LOX from Glycinemax in 25 mM borate buffer pH 9 in the presence of 200 μM DTPA, 0.05% sodium cholate, 5 μM H2O2 at RT for

45 min. Incubation mixture was continuously bubbled with 95% O2. At the end of incubation PE-OOH was extracted and purified by HPLC (Shimadzu Corp.) using 4.4×150 mm 5 μm C18 column (Phenomenex). Isocratic mobile phase consists of acetonitrile/water/triethylamine/acetic acid - 900/100/5/5 v/v was used for separation. Purity was confirmed by LC/MS using LQX ion trap mass spectrometer (ThermoFisher Scientific). Purified PE-OOH (99%) was reconstituted in DMSO and added to cells.

Identification of PE oxygenated products in cell lysates

WT Pfal1 cells were treated with RSL3 (100 nM) for 6 hrs. Cells were re-suspended in 25 mM HEPES buffer (pH 7.4) containing 200 μM DTPA, sonicated and used for the experiment. 1-steraoyl-2-arachidonoyl-PE was added to cell lysates (10 nmol/3×10^6 cells) and incubated at 37° C for 2 hrs in the absence and in the presence of human recombinant 15-LOX from Glycinemax. In separated series of the experiment cell lysates were incubated in the presence of 1-steraoyl-2-arachidonoyl-hydroperoxy-PE (10 nmol/3×10^6 cells) for 2 hrs and at 37° C. At the end of incubation lipids were extracted and oxygenated PE products were identified by MS/MS analysis using an Orbitrap Fusion Lumos mass spectrometer (ThermoFisher Scientific). The instrument was operated with electrospray ionization probe in negative polarity mode. Ion source conditions were set as follows: Spray voltage = 3 kV, Sheath gas = 55 (arbitrary unit), Auxiliary gas = 10 (arb. unit), Sweep gas = 0.5 (arb. unit), Transfer tube temperature = 300 °C, Vaporizer temperature = 200 °C, RF-Lens level = 20 %. Data were acquired in data-dependant-MS^2 targeted-MS^3 mode with Cycle Time setting of 3 s. For MS scan event, the parameters were set as follow: Ion detection = Orbitrap, Mass resolution = 120,000, Scan range = m/z 400 – 1800, AGC target = 1e5. The most intense ion was selected for the data-dependent MS^2 scan. Dynamic exclusion = 9 s. Exclusion mass list for MS^2 (m/z values of 130 background ions) was created from a solvent blank injection data. For MS^2 scan event(s), the parameters were set as follows: Quadrupole isolation = 1 Da, First Mass = m/z 87, Activation type = HCD, Collision energy = 28 % with step 8 %, Ion detection = Orbitrap, Mass resolution = 15,000, Max Injection time = 250 ms, AGC target = 2e4. Product ions from a targeted mass list were selected for MS^3 scan. Target mass list for MS^3: 319.2279, 317.2123, 335.2228, 333.2072, 317.2123, 351.2159, 333.2054, 349.2003, 331.1898, 367.2126, 349.2021, 331.1916. For MS^3 scan event(s), the parameters were set as follows: Top N = 4, Isolation window = 2 Da, Activation type = HCD, Collision energy = 40 %, Ion detection = Ion Trap, Ion trap Scan rate = Rapid, Max Injection time = 500 ms, AGC target = 3e4.

Oxygenation of SAPE and SAPC

Liposomes containing SAPE and SAPC (ratios 1:1 and 1:4) were incubated with recombinant human 15-LOX-2 (2U/ml) in 25 mM borate buffer (pH 7.8) containing 0.003% tween, 100 μM DTPA for 30 min at room temperature with constant oxygen bubbling. Samples were extracted with chloroform/methanol and LC/MS analysis was performed as described above.

Determination of long-chain acyl-CoAs

Long-chain acyl-CoAs were extracted from the collected cells with chloroform/ethanol mixture[46] and then isolated with 2-(2-pyridyl) ethyl- functionalized silica gel SPE cartridges

(Supelco)[47]. The contents of molecular species of long-chain acyl-CoAs were determined by LC/MS[48].

Arachidonoyl-CoA oxidation

Exhaustive oxidation of arachidonoyl-CoA by human recombinant 15-LOX-2 was performed at 21°C for 60 min in the presence of 1.2 μM H2O2 plus 0.3 mM CaCl2 in 25 mM HEPES buffer containing 100 M DTPA (pH=7.4).

LC-MS analysis of phospholipids and fatty acids

Lipids were extracted by using Folch procedure[49] and phospholipids and fatty acids were further analyzed by LC-MS/MS using normal phase (silica) or reverse phase (C18) chromatography followed by MS and MS/MS analysis on a Q-Exactive hybrid-quadrupole-orbitrap mass spectrometer (ThermoFisher Scientific).

Identification of PEox in cells

PE fraction (containing both non-oxygenated and oxygenated PE) was obtained from WT cells treated with AA and exposed to RSL3 by normal phase LC/MS. PE and PEox (PE-OOH) were separated on a reverse phase column (Luna 3 μm C8 (2) 100A, 150 × 4.6 mm (Phenomenex). The column was maintained at room temperature. The analysis was performed using an isocratic solvent system consisting of acetonitrile/H2O/trimethylamine/acetic acid (45/5/0.5/0.5, v/v/v/v). All solvents were LC/MS grade. The column was eluted at a flow rate of 1.5 ml/min and the eluant was monitored by UV absorbance at 205 and 235nm on a Shimadzu HPLC system (Shimadzu Corp.). Fractions containing PEox were collected and identification was confirmed by mass spectrometry.

LC-MS analysis of free and esterified fatty acids

Lipids were extracted by using Folch procedure[49]. Oxygenated free fatty acids were obtained from total lipids by solid phase extraction (SPE) using OASIS HLB 1cc (30 mg) extraction cartridges (Waters Corp.) as described[50]. To liberate esterified oxygenated fatty acids, lipid extracts were treated with pletelet-activating factor-acetylhydrolase (PAF-AH) (0.01 units/100 nmol of phospholipids, 45 min at 37°C in HEPES buffer pH 7.4). Liberated oxygenated fatty acids were extracted by SPE and analyzed by reverse phase LC/MS (see below).

Normal phase column separation of phospholipids

Phospholipids were separated on a normal phase column (Luna 3 μm Silica (2) 100Å, 150 × 2.0 mm, (Phenomenex)) at a flow rate of 0.2 mL/min on a Dionex Ultimate 3000 HPLC system. The column was maintained at 35°C. The analysis was performed using gradient solvents (A and B) containing 10 mM ammonium acetate and 0.5% triethylamine. Solvent A contained propanol:hexane:water (285:215:5, v/v/v) and solvent B contained propanol:hexane:water (285:215:40, v/v/v). All solvents were LC/MS grade. The column was eluted for 0.5 min isocratically at 25% B, then from 0.5 to 6.5 min with a linear gradient from 25% to 40% solvent B, from 6.5–25 min using a linear gradient of 40–55% solvent B, from 25–38 min with a linear gradient of 55–70% solvent B, from 38–48 min using a linear

gradient of 70%–100% solvent B, then isocratically from 48–55 min at 100% solvent B followed by a return to initial conditions from 55–70 min from 100% to 25% B. The column was then equilibrated at 25%B for an additional 5 min.

Reverse phase column separation of fatty acids

Fatty acids were separated on a reverse phase column (Luna 3 μm C18 (2) 100Å, 150 × 1.0 mm, (Phenomenex) at a flow rate of 0.050 mL/min. The column was maintained at 35°C. The analysis was performed using gradient solvents (A and B) containing 10mM ammonium acetate. Solvent A contained methanol/H2O/acetonitrile (10/85/5, v/v/v). Solvent B contained methanol/H2O/acetonitrile/propanol (90/5/5/0.5, v/v/v/v). All solvents were LC/MS grade. The column was eluted for 0.5min at 50%B, from 0.5 to 2.5 min with a linear gradient from 50% to 75% solvent B, then isocratically from 2.5–10 min at 75% solvent B, then 10–15 min with a linear gradient from 75% to 100% solvent B, then isocratically at 100% B from 15–20 min. At 21 min, the column was returned to starting conditions (50% solvent B) and held at this condition for an additional 9 min.

MS and MS/MS analysis of phospholipids

MS and MS/MS analysis of PLs was performed on a Q-Exactive hybrid-quadrupole-orbitrap mass spectrometer (ThermoFisher Scientific). Analysis was performed in negative ion mode at a resolution of 140,000 for the full MS scan and 17,500 for the MS^2 scan in a data-dependent mode. The scan range for MS analysis was 400–1800 m/z with a maximum injection time of 128 ms using 1 microscan. A maximum injection time of 500 ms was used for MS^2 (high energy collisional dissociation (HCD)) analysis with collision energy set to 24 with an inclusion list for phospholipids including PE, PC and CL and their oxidized and deuterated products. An isolation window of 1.0 Da was set for the MS and MS^2 scans. Capillary spray voltage was set at 3.5 kV, and capillary temperature was 320 OC. The S-lens Rf level was set to 60.

MS and MS/MS analysis of fatty acids

MS and MS/MS analysis of PLs was performed on a Q-Exactive hybrid-quadrupole-orbitrap mass spectrometer (ThermoFisher Scientific). Analysis was performed in negative ion mode at a resolution of 140,000 for the full MS scan and 17,500 for the MS^2 scan in a data-dependent mode. The scan range for MS analysis was 150–500 m/z with a maximum injection time of 100 ms using 1 microscan. A maximum injection time of 100 ms was used for MS^2 (high energy collisional dissociation (HCD)) analysis with collision energy set to 30 with an inclusion list for fatty acids, fatty acid metabolites and their oxidized and deuterated products. An isolation window of 1.0 Da was set for the MS and MS^2 scans. Capillary spray voltage was set at 3.2 kV, and capillary temperature was 320 OC. The S-lens Rf level was set to 65.

Detection of tocopherols and oxidized AA by LC/MS

Reaction conditions: 20 μM AA acid is incubated at 37°C with 2.8 mU of 15-LOX and 10 μM of each inhibitor in 50 mM Tris-HCl buffer (pH 7.4) for 5 minutes. The reactions were stopped by adding 9 times excess of acetonitrile. For oxidized AA analysis 1 μM internal

standard is added to the above mixture and analyzed through LC-MS as described previously[51]. Vitamin E was extracted by Folch procedure[49] and LC-ESI-MS analysis was performed on a Dionex LC system (UltiMate 3000 autosampler) coupled to an LXQ ion trap mass spectrometer with the Xcalibur operating system, (ThermoFisher Scientific). The instrument was operated in the positive ion mode at 5.0 kV. The source temperature was maintained at 175 °C. Spectra were acquired using full range zoom (m/z 200−600) scans. Tocopherol and its analogs were separated on a reverse phase column Luna 3 μm C18 (2) 100A, 150 mm × 1 mm (Phenomenex) at a flow rate of 0.065 mL/min. The column was maintained at 30 °C. The analysis was performed using gradient solvents (A and B). Solvent A consisted methanol/water (1:1) containing 5 mM ammonium acetate. Solvent B consisted of methanol containing 0.1 % NH4. The column was eluted during the first 5 min isocratically at 65 % solvent B, from 5 to 10 min with a linear gradient from 65 to 95% solvent B, from 10 to 20 min with a linear gradient from 95 to 100, from 20 to 25 min isocratically using 100 % solvent B, from 25 to 30 min with a linear gradient from 100 to 65 % solvent B, and from 30 to 35 min isocratically using 65% solvent B for equilibration of the column.

Detection of Tocopherol phenoxyl radicals by ESR spectroscopy

Reaction conditions and ESR spectrometer settings: ESR spectrometer (JEOL JES-FA100) settings were center field 335.5 mT, scan range 10 mT, scan sweep 10 mT/min (10 scans), time constant 0.1 s, magnetic field 100 kHz, modulation amplitude 0.2 mT, microwave frequency 9.44 GHz, microwave power 50 mW, receiver gain 5×10^3 and at 25°C. Phenoxyl radicals of α-Tocopherol and its analogs (3 mM) were generated by 15-LOX (2.5 KU) in the presence of arachidonic acid (1 mM) in PBS pH 7.4, deoxycholic acid sodium salt (0.1 %) and DTPA (100 μM).

Molecular docking

The molecular docking modeling was employed to study the interactions of free/esterified fatty acids and vitamin E family molecules with human 15LOX-2 (based on PDB ID: 4NRE[52]). The small molecules —lipids or inhibitors—were docked to the proteins using AutoDock Vina program, version 1.1.2 (http://vina.scripps.edu). The lipids, the inhibitors and the protein structures were converted from pdb into pdbqt format using MGL Tools (http://mgltools.scripps.edu). Due the large size of 15-LOX-2 protein we applied a large grid box for the docking modeling. We used grid boxes with dimensions of 112 × 102 × 72 Å. Three docking modeling were run using three different random number generator seeds, with the exhaustiveness set at 14 to obtain a higher accuracy to find the binding site and reduce the discrepancies among the binding affinities. The best model was selected among those models, in which the small molecule was bound at the catalytic site of 15-LOX-2 with the highest binding affinity (the lowest binding energy).

Coarse-grained molecular dynamics (CGMD) simulations

CGMD simulations were based on the MARTINI force field for biomolecular simulations[53]. CGMD simulations were applied to study the interactions of 15-LOX-2 with the membrane comprises PC and PE. Protein was located in ~20 Å distance from the membrane surface with different orientations. The position of protein was restricted during equilibration runs.

A 15 fs time step was used to integrate the equations of motion. Analysis of the final configuration of the CGMD runs revealed the preferred PL substrate. All simulations were performed using the GROMACS v. 4.5.4 MD package[54] and visualized using VMD v. 1.9 software (http://www.ks.uiuc.edu/Research/vmd/). Initially, each system was minimized for 20 ps, before 1 ns NVT and 1 ns NPT ensemble equilibration. A 15 fs time step was used to integrate the equations of motion. Non-bonded interactions have a cutoff distance of 1.2 nm. Simulations were run at 310 K and at 1 atm during NPT runs.

Mathematical Modeling

We constructed the phospholipid metabolic network regulating ferroptosis based on our data presented in this manuscript, literature[55,56] and the Reactome and KEGG databases. The reaction scheme of the network is shown in Supplementary Fig. 16a. All acronyms used are listed in Supplementary Table 3. A system of ODEs derived from the reaction network is described in detail in below. Simulations and sensitivity analysis were performed using COPASI tool[57] with the LSODA solver.

Here we briefly describe the three modules in our network model:

AA metabolism - The release of AA from membrane phospholipids can be catalyzed by enzymes such as PLA2. The free AA is oxidized to 5-HPETE, 12-HPETE and 15-HPETE by 5-LOX, 12-LOX and 15-LOX respectively, which are reduced to 5-HETE, 12-HETE and 15-HETE by GPX4, in the presence of GSH. 5-LOX further converts 5-HETE into LTA4. AA is also oxidized by COX to produce PGH2, which leads to the production of lipid mediators including PGE2. The feedback reactions involving 5/12/15-HPETE, 5/12/15-HETE, LTA4, and PGE2 were based on the literature[55,56].

AA induced ferroptosis - Acsl4 catalyzes the formation of AA-CoA. Elongase elongate AA-CoA to AdA-CoA. AA-CoA and AdA-CoA can either be broken down via beta oxidation or be esterified into PE to form PE-AA and PE-AdA catalyzed by Lcat3. LOXes convert PE-AA and PE-AdA into PE-AA-OOH and PE-AdA-OOH. The accumulation of PE-AA-OOH and PE-AdA-OOH leads to ferroptotic cell death.

GPX4 dependent regulation -System x_c^- imports Cys and exports Glu. GCS catalyzes the formation of Cys-Glu, which reacts with Gly and forms GSH catalyzed by GS. GSH is converted into GSSG by GPX4, while PE-AA-OOH and PE-AdA-OOH are reduced into PE-AA-OH and PE-AdA-OH. GR catalyzes the conversion from GSSG to GSH.

The dynamics of the network was modeled as a system of 47 ordinary differential equations (ODEs) (Supplementary Table 4). The reaction rates for catalysis are described using Michaelis-Menten kinetics. For example, the equation below shows an enzyme catalytic reaction

$$S+E \xrightarrow{v} P+E$$

where S denotes substrate, E denote enzyme, P denotes product, and v is the reaction rate. The kinetics of the reaction is modeled as:

$$v=\frac{K_{cat}\cdot S\cdot E}{K_m+S}$$

where K_{cat} is the turnover number and Km is the Michaelis-Menton constant. The rate equation for the catalysis involves two substrates S_1 and S_2 is:

$$v=\frac{K_{cat}\cdot S_1\cdot S_2\cdot E}{K_{m1}\cdot K_{m2}+K_{m1}\cdot S_1+K_{m2}\cdot S_2+S_1\cdot S_2}$$

The rate equation for the catalysis involves inhibitors I_1, I_2, … is:

$$v=\frac{K_{cat}\cdot S\cdot E}{K_m\left(1+\frac{I_1}{K_{i1}}+\frac{I_2}{K_{i2}}+\cdots\right)+S}$$

The rate equation for the catalysis involves activators A_1, A_2, … is:

$$v=\frac{K_{cat}\cdot S\cdot E\cdot\left(1+\frac{A_1}{K_{a1}}+\frac{A_2}{K_{a2}}+\cdots\right)}{K_m+S}$$

The reaction rates for transcriptional regulation and decay are modeled using Hill equation and mass law kinetics respectively.

We defined a score indicating cell death signal strength as a linear combination of the concentrations of PE-AA-OOH and PE-AdA-OOH:

$$S_{death}=\alpha+\beta_1\cdot[\mathrm{PE-AA-OOH}]+\beta_2\cdot[\mathrm{PE-AdA-OOH}]$$

where α is the basal level of cell death, β_1 and β_2 are coefficients. We then use the integration of S_{death} over time to predict cell death level.

We used the experimental data obtained to calibrate model parameters including initial concentrations of species and reaction rate constants. Specifically, we used the data shown in Figure 1C to establish the relationship between RSL3 pretreatment time and GPX-4 initial concentration. We then estimated the unknown parameters by fitting the experimental data of ferroptotic cell death levels under different conditions. The model was further validated using an independent test data set. The comparison and model predictions and experimental data are shown in Supplementary Fig. 16, b–i. The resulting parameters are shown in Supplementary Table 5.

Statistical Analysis

The data are presented as mean ± s.d. values from at least three experiments. Statistical analyses were performed by either unpaired Student's t-test or one-way ANOVA. The statistical significance of differences was set at $p<0.05$. Phospholipids were quantified from

the full scan LC/MS spectra with ratiometric comparison to the pre-selected internal standard using corresponding standard curve for each phospholipid class. Differences between the groups were analyzed by one-way ANOVA with Tukey post-hoc analyses by SPSS 18.0 software (SPSS Inc). Orthogonal partial least squares discriminant analysis (OPLS-DA), a multivariate analysis method was used to discriminate between live and ferroptotic cells using SIMCA 13.0 software (Umetrics). The criteria for confirming a potential biomarker were: 1) variable importance in projection (VIP) greater than one, 2) jack knife uncertainty bar excluding zero, 3) absolute value of Pcorr in the S-plot greater than 0.58.

Supplementary Material

Refer to Web version on PubMed Central for supplementary material.

Acknowledgments

Supported by NIH (P01HL114453, U19AI068021, NS076511, NS061817, ES020693), and HFSP-RGP0013/2014.This work was in part supported by grants from the Deutsche Forschungsgemeinschaft (DFG) CO 291/2-3 and CO 291/5-1 to M.C. We are thankful to Dr. J. Ruzicka (ThermoFisher Scientific) for help in obtaining MS^3 spectra of PE oxidation products using tribrid Fusion Lumos (ThermoFisher Scientific),

References

1. Allocati N, Masulli M, Di Ilio C, De Laurenzi V. Die for the community: an overview of programmed cell death in bacteria. Cell Death Dis. 2015; 6:e1609. [PubMed: 25611384]
2. Byrne JM, et al. Redox cycling of Fe(II) and Fe(III) in magnetite by Fe-metabolizing bacteria. Science. 2015; 347:1473–6. [PubMed: 25814583]
3. Dixon SJ, Stockwell BR. The role of iron and reactive oxygen species in cell death. Nat Chem Biol. 2014; 10:9–17. [PubMed: 24346035]
4. Dixon SJ, et al. Ferroptosis: an iron-dependent form of nonapoptotic cell death. Cell. 2012; 149:1060–72. [PubMed: 22632970]
5. Yang WS, Stockwell BR. Ferroptosis: Death by Lipid Peroxidation. Trends Cell Biol. 2016; 26:165–76. [PubMed: 26653790]
6. Yang WS, Stockwell BR. Synthetic lethal screening identifies compounds activating iron-dependent, nonapoptotic cell death in oncogenic-RAS-harboring cancer cells. Chem Biol. 2008; 15:234–45. [PubMed: 18355723]
7. Imai H, Nakagawa Y. Biological significance of phospholipid hydroperoxide glutathione peroxidase (PHGPx, GPx4) in mammalian cells. Free Radic Biol Med. 2003; 34:145–69. [PubMed: 12521597]
8. Yamanaka K, et al. A novel fluorescent probe with high sensitivity and selective detection of lipid hydroperoxides in cells. RSC Advances. 2012; 2:7894–7900.
9. Drummen GP, van Liebergen LC, Op den Kamp JA, Post JA. C11-BODIPY(581/591), an oxidation-sensitive fluorescent lipid peroxidation probe: (micro)spectroscopic characterization and validation of methodology. Free Radic Biol Med. 2002; 33:473–90. [PubMed: 12160930]
10. Li B, Pratt DA. Methods for determining the efficacy of radical-trapping antioxidants. Free Radic Biol Med. 2015; 82:187–202. [PubMed: 25660993]
11. Kuch EM, et al. Differentially localized acyl-CoA synthetase 4 isoenzymes mediate the metabolic channeling of fatty acids towards phosphatidylinositol. Biochim Biophys Acta. 2014; 1841:227–39. [PubMed: 24201376]
12. Golej DL, et al. Long-chain acyl-CoA synthetase 4 modulates prostaglandin E(2) release from human arterial smooth muscle cells. J Lipid Res. 2011; 52:782–93. [PubMed: 21242590]
13. Doll S, et al. Acsl4 Dictates Ferroptosis Sensitivity by Shaping Cellular Lipid Composition. Nat Chem Biol. 2016

14. McIntyre TM, Prescott SM, Stafforini DM. The emerging roles of PAF acetylhydrolase. J Lipid Res. 2009; 50(Suppl):S255–9. [PubMed: 18838739]
15. Soh N, et al. Swallow-tailed perylene derivative: a new tool for fluorescent imaging of lipid hydroperoxides. Org Biomol Chem. 2007; 5:3762–8. [PubMed: 18004455]
16. Dixon SJ, et al. Human Haploid Cell Genetics Reveals Roles for Lipid Metabolism Genes in Nonapoptotic Cell Death. ACS Chem Biol. 2015; 10:1604–9. [PubMed: 25965523]
17. Seiler A, et al. Glutathione peroxidase 4 senses and translates oxidative stress into 12/15-lipoxygenase dependent- and AIF-mediated cell death. Cell Metab. 2008; 8:237–48. [PubMed: 18762024]
18. Friedmann Angeli JP, et al. Inactivation of the ferroptosis regulator Gpx4 triggers acute renal failure in mice. Nat Cell Biol. 2014; 16:1180–91. [PubMed: 25402683]
19. Askari B, et al. Rosiglitazone inhibits acyl-CoA synthetase activity and fatty acid partitioning to diacylglycerol and triacylglycerol via a peroxisome proliferator-activated receptor-gamma-independent mechanism in human arterial smooth muscle cells and macrophages. Diabetes. 2007; 56:1143–52. [PubMed: 17259370]
20. O'Donnell VB, Murphy RC. New families of bioactive oxidized phospholipids generated by immune cells: identification and signaling actions. Blood. 2012; 120:1985–92. [PubMed: 22802337]
21. Xiao Y, Guengerich FP. Metabolomic analysis and identification of a role for the orphan human cytochrome P450 2W1 in selective oxidation of lysophospholipids. J Lipid Res. 2012; 53:1610–7. [PubMed: 22591743]
22. Khanna S, et al. Molecular basis of vitamin E action: tocotrienol modulates 12-lipoxygenase, a key mediator of glutamate-induced neurodegeneration. J Biol Chem. 2003; 278:43508–15. [PubMed: 12917400]
23. Arai H, Nagao A, Terao J, Suzuki T, Takama K. Effect of d-alpha-tocopherol analogues on lipoxygenase-dependent peroxidation of phospholipid-bile salt micelles. Lipids. 1995; 30:135–40. [PubMed: 7769969]
24. Dennis EA. Diversity of group types, regulation, and function of phospholipase A2. J Biol Chem. 1994; 269:13057–60. [PubMed: 8175726]
25. van den Brink-van der Laan E, Killian JA, de Kruijff B. Nonbilayer lipids affect peripheral and integral membrane proteins via changes in the lateral pressure profile. Biochim Biophys Acta. 2004; 1666:275–88. [PubMed: 15519321]
26. Lee AG. How lipids affect the activities of integral membrane proteins. Biochim Biophys Acta. 2004; 1666:62–87. [PubMed: 15519309]
27. Toppo S, Flohe L, Ursini F, Vanin S, Maiorino M. Catalytic mechanisms and specificities of glutathione peroxidases: variations of a basic scheme. Biochim Biophys Acta. 2009; 1790:1486–500. [PubMed: 19376195]
28. Uderhardt S, et al. 12/15-lipoxygenase orchestrates the clearance of apoptotic cells and maintains immunologic tolerance. Immunity. 2012; 36:834–46. [PubMed: 22503541]
29. Orrenius S, Zhivotovsky B. Cardiolipin oxidation sets cytochrome c free. Nat Chem Biol. 2005; 1:188–9. [PubMed: 16408030]
30. Kagan VE, et al. Cytochrome c acts as a cardiolipin oxygenase required for release of proapoptotic factors. Nat Chem Biol. 2005; 1:223–32. [PubMed: 16408039]
31. Massey KA, Nicolaou A. Lipidomics of polyunsaturated-fatty-acid-derived oxygenated metabolites. Biochem Soc Trans. 2011; 39:1240–6. [PubMed: 21936796]
32. Kuhn H, Banthiya S, van Leyen K. Mammalian lipoxygenases and their biological relevance. Biochim Biophys Acta. 2015; 1851:308–30. [PubMed: 25316652]
33. Schroeder F. Regulation of aminophospholipid asymmetry in murine fibroblast plasma membranes by choline and ethanolamine analogues. Biochim Biophys Acta. 1980; 599:254–70. [PubMed: 6249356]
34. Sessions A, Horwitz AF. Myoblast Aminophospholipid Asymmetry Differs from That of Fibroblasts. Febs Letters. 1981; 134:75–78. [PubMed: 9222328]
35. Garreta A, et al. Structure and interaction with phospholipids of a prokaryotic lipoxygenase from Pseudomonas aeruginosa. FASEB J. 2013; 27:4811–21. [PubMed: 23985801]

36. Suardiaz R, et al. Understanding the Mechanism of the Hydrogen Abstraction from Arachidonic Acid Catalyzed by the Human Enzyme 15-Lipoxygenase-2. A Quantum Mechanics/Molecular Mechanics Free Energy Simulation. J Chem Theory Comput. 2016; 12:2079–90. [PubMed: 26918937]
37. Noguchi N, et al. The specificity of lipoxygenase-catalyzed lipid peroxidation and the effects of radical-scavenging antioxidants. Biol Chem. 2002; 383:619–26. [PubMed: 12033451]
38. Carlson BA, et al. Glutathione peroxidase 4 and vitamin E cooperatively prevent hepatocellular degeneration. Redox Biol. 2016; 9:22–31. [PubMed: 27262435]
39. Chen L, Hambright WS, Na R, Ran Q. Ablation of the Ferroptosis Inhibitor Glutathione Peroxidase 4 in Neurons Results in Rapid Motor Neuron Degeneration and Paralysis. J Biol Chem. 2015; 290:28097–106. [PubMed: 26400084]
40. Matsushita M, et al. T cell lipid peroxidation induces ferroptosis and prevents immunity to infection. J Exp Med. 2015; 212:555–68. [PubMed: 25824823]
41. Wortmann M, et al. Combined deficiency in glutathione peroxidase 4 and vitamin E causes multiorgan thrombus formation and early death in mice. Circ Res. 2013; 113:408–17. [PubMed: 23770613]
42. Sen CK, Khanna S, Roy S, Packer L. Molecular basis of vitamin E action. Tocotrienol potently inhibits glutamate-induced pp60(c-Src) kinase activation and death of HT4 neuronal cells. J Biol Chem. 2000; 275:13049–55. [PubMed: 10777609]
43. Yang WS, et al. Regulation of ferroptotic cancer cell death by GPX4. Cell. 2014; 156:317–31. [PubMed: 24439385]

Reference for Online Methods

44. Telmer CA, et al. Rapid, specific, no-wash, far-red fluorogen activation in subcellular compartments by targeted fluorogen activating proteins. ACS Chem Biol. 2015; 10:1239–46. [PubMed: 25650487]
45. Szent-Gyorgyi C, et al. Fluorogen-activating single-chain antibodies for imaging cell surface proteins. Nat Biotechnol. 2008; 26:235–40. [PubMed: 18157118]
46. Tardi PG, Mukherjee JJ, Choy PC. The quantitation of long-chain acyl-CoA in mammalian tissue. Lipids. 1992; 27:65–7. [PubMed: 1608307]
47. Minkler PE, Kerner J, Ingalls ST, Hoppel CL. Novel isolation procedure for short-, medium-, and long-chain acyl-coenzyme A esters from tissue. Anal Biochem. 2008; 376:275–6. [PubMed: 18355435]
48. Sun D, Cree MG, Wolfe RR. Quantification of the concentration and 13C tracer enrichment of long-chain fatty acyl-coenzyme A in muscle by liquid chromatography/mass spectrometry. Anal Biochem. 2006; 349:87–95. [PubMed: 16307720]
49. Folch J, Lees M, Sloane Stanley GH. A simple method for the isolation and purification of total lipides from animal tissues. J Biol Chem. 1957; 226:497–509. [PubMed: 13428781]
50. Miller TM, et al. Rapid, simultaneous quantitation of mono and dioxygenated metabolites of arachidonic acid in human CSF and rat brain. J Chromatogr B Analyt Technol Biomed Life Sci. 2009; 877:3991–4000.
51. Tejero J, et al. Peroxidase activation of cytoglobin by anionic phospholipids: Mechanisms and consequences. Biochim Biophys Acta. 2016; 1861:391–401. [PubMed: 26928591]
52. Kobe MJ, Neau DB, Mitchell CE, Bartlett SG, Newcomer ME. The structure of human 15-lipoxygenase-2 with a substrate mimic. J Biol Chem. 2014; 289:8562–9. [PubMed: 24497644]
53. Marrink SJ, Risselada HJ, Yefimov S, Tieleman DP, de Vries AH. The MARTINI force field: coarse grained model for biomolecular simulations. J Phys Chem B. 2007; 111:7812–24. [PubMed: 17569554]
54. Van der Spoel D, et al. GROMACS: Fast, flexible, and free. Journal of Computational Chemistry. 2005; 26:1701–1718. [PubMed: 16211538]
55. Yang K, et al. Dynamic simulations on the arachidonic acid metabolic network. PLoS Comput Biol. 2007; 3:e55. [PubMed: 17381237]

56. Gupta S, Maurya MR, Stephens DL, Dennis EA, Subramaniam S. An integrated model of eicosanoid metabolism and signaling based on lipidomics flux analysis. Biophys J. 2009; 96:4542–51. [PubMed: 19486676]

57. Hoops S, et al. COPASI–a COmplex PAthway SImulator. Bioinformatics. 2006; 22:3067–74. [PubMed: 17032683]

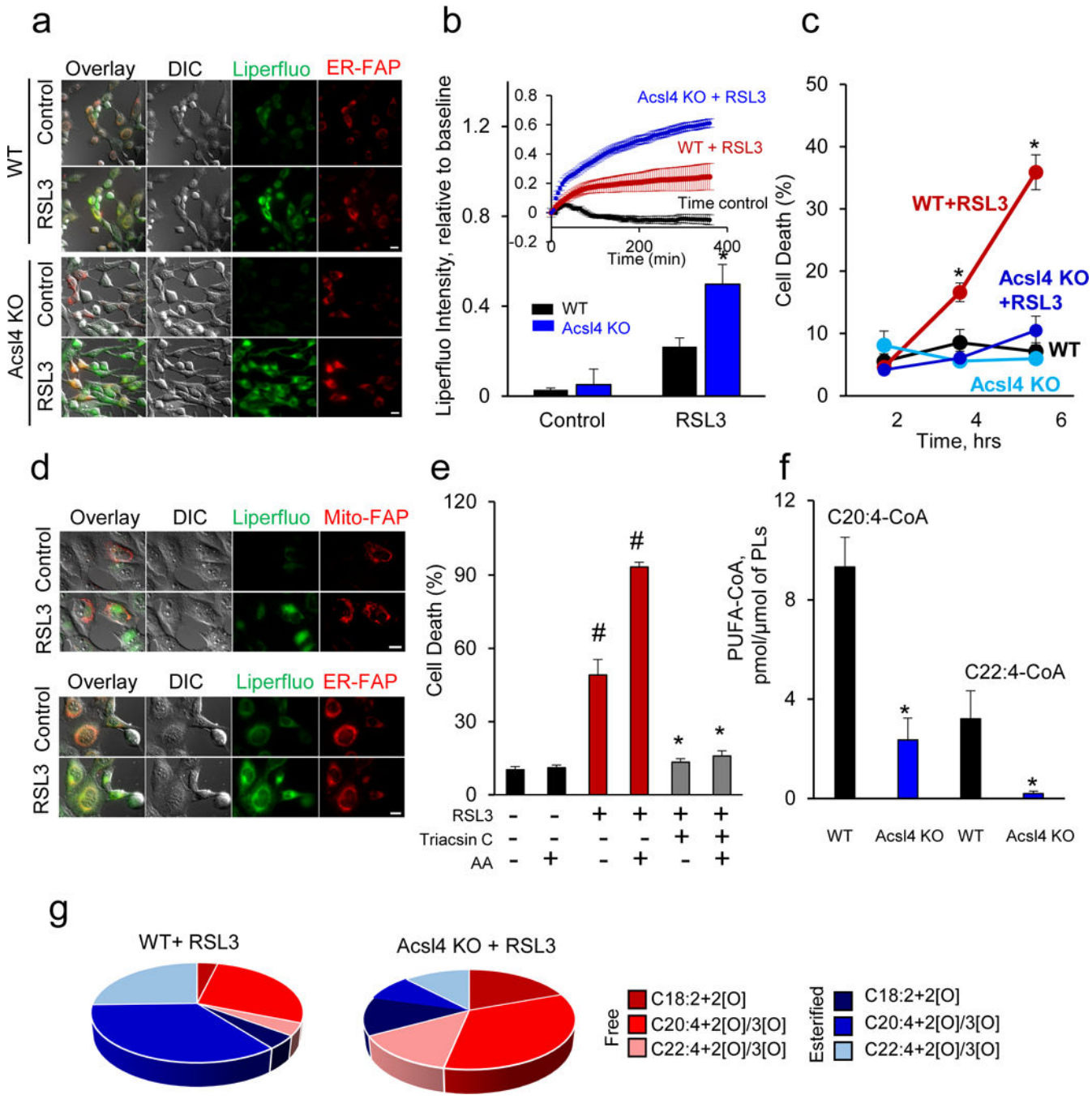

Figure 1. Oxygenation of esterified (but not free) AA contributes to RSL3-induced ferroptosis in WT and Acsl4 KO Pfa1 cells

(**a**) Live cell fluorescence imaging of lipid hydroperoxides in WT and Acsl4 KO cells treated with RSL3 (100 nM, 6 hrs, scale bar 5 µm). (**b**) LiperFluo fluorescence intensity following RSL3 treatment in WT and Acsl4 KO cells. Insert: Fluorescence time course after RSL3 treatment (100 nM) in WT and Acsl4 KO cells with a time control. The data were from a minimum of 10 stage positions. For the statistical analysis, each stage position counted as one data entry. *$P < 0.05$ *vs.* WT+RSL3 cells (t-test). (**c**) WT and Acsl4 KO cells were

treated with RSL3 (100 nM) for 2, 4, and 6 hrs before cell death analysis. Data are mean ± s.d., n=3. *$P < 0.05$ *vs.* ACSL4 KO+RSL3 (t-test). (**d**) Fluorescence responses from Mito-FAP (red, upper panel) and ER-FAP (red, lower panel) *vs.* LiperFluo (green, both panels, scale bars 5 μm). (**e**) ACSL inhibitor, Triacsin C, suppresses ferroptosis in Pfa1 cells. AA (2.5 μM,16 hrs); RSL3 (100 nM, 6 hrs); Triacsin C (2.5 μM, 6 hrs). Data are mean ± s.d., n=3. *$P < 0.05$ *vs.* control (t-test). (**f**) Contents of AA-CoA and AdA-CoA in WT and Acsl4 KO cells. Data are mean ± s.d., n=3. *$P < 0.05$ *vs.* WT cells (t-test). (**g**) Distribution of free and esterified PUFA-OOH in WT and Acsl4 KO Pfa1 cells treated with RSL3 (100 nM, 6 hrs).

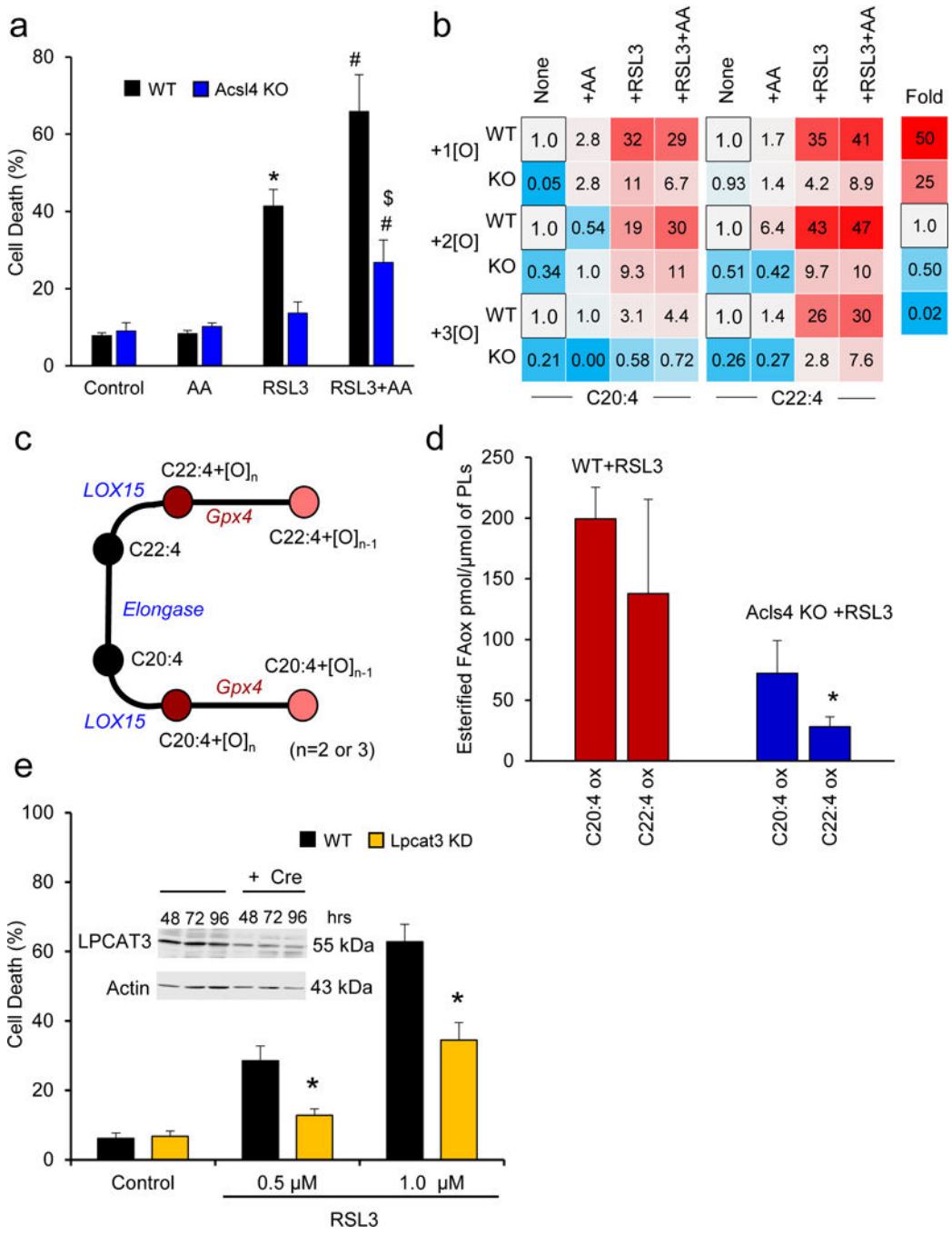

Figure 2. Effects of exogenous AA on RSL3-triggered ferroptosis

(**a**) WT and Acsl4 KO cells were pretreated with AA (2.5 μM, 16 hrs) followed by RSL3 (100 nM, 6 hrs). Data are mean ± s.d., n=3; *,#,$ indicate $P < 0.05$ *vs.* control, RSL3 (or Acsl4 KO+RSL3), RSL3+AA, respectively (t-test). (**b**) LC-MS based heat maps for oxygenated esterified AA (C20:4) and AdA (C22:4) (normalized to corresponding WT group, in black), showing their relative changes after different treatments. (**c**) Schema of metabolic pathways for C20:4, C22:4 and their oxygenated products. (**d**) Levels of oxidized AA and AdA esterified into phospholipids in WT and Acsl4 KO Pfa1 cells. Data are mean ±

s.e.m., n=3. *$P < 0.05$ *vs.* WT cells (one-tailed t-test). (**e**) Lpcat3 KD decreased RSL3-induced ferroptosis in MLE cells. Data are mean ± s.d., n=3. *$P < 0.05$ *vs.* WT cells (t-test). Insert: LPCAT3 decrease was confirmed by western blotting (48, 72 and 96 hrs) after Cre addition (for the full blot, see Supplementary Fig. 18a).

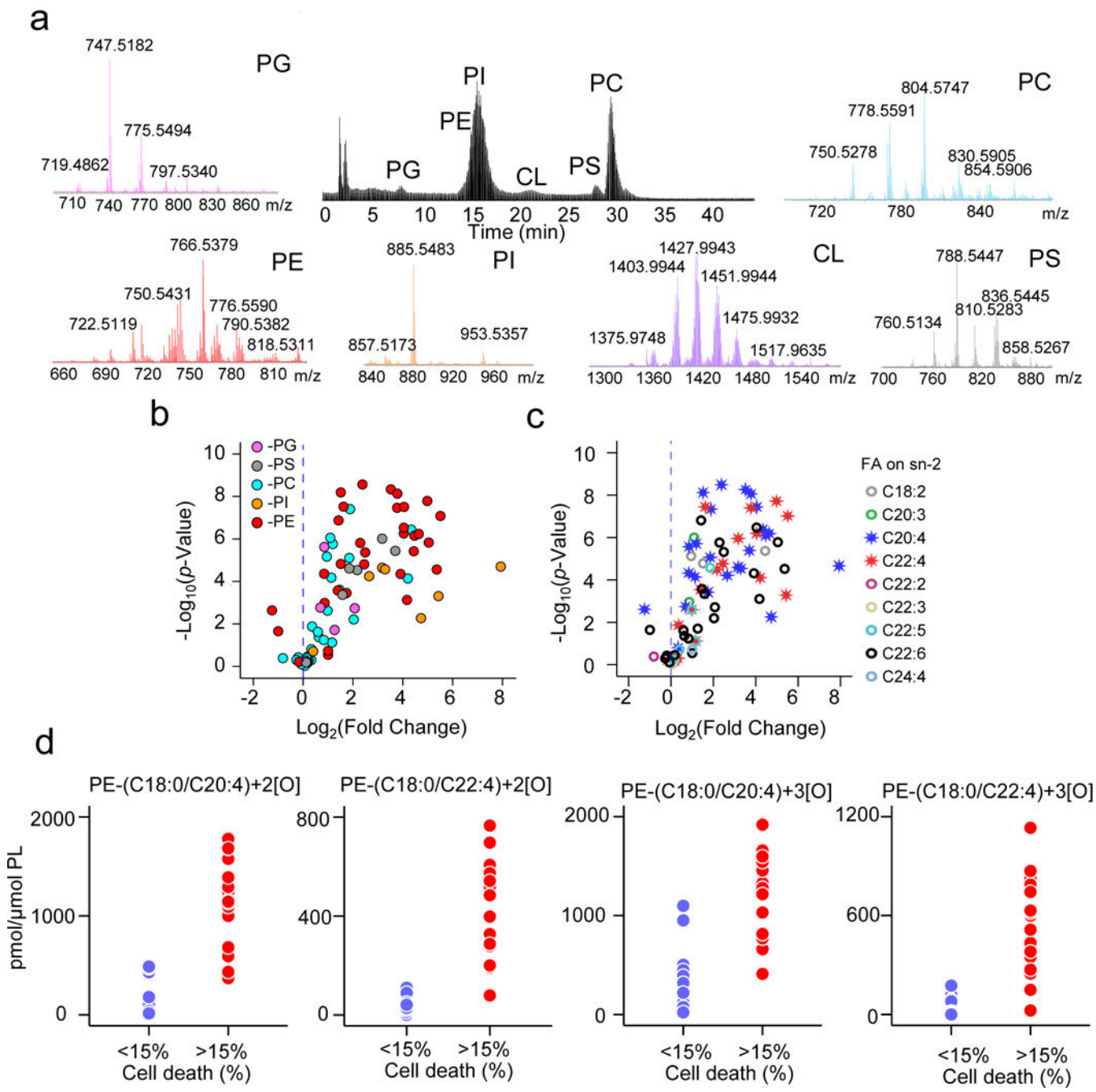

Figure 3. Screening of phospholipids and their oxidation products identifies ferroptosis death signals

(**a**) Representative normal phase LC-MS/MS chromatogram and mass spectra for six major classes of phospholipids in Pfa1 cells. (**b**) Scatter plot of RSL3 induced changes in the levels of oxygenated phospholipids (log2 (fold-change), X-axis) *vs.* significance (−log10 (*p*-Value), Y-axis, by *t*-test) of live (cell death <15%, number of replicate data points is 26) and ferroptotic cells (cell death >15%, number of replicate data points is 18). No oxygenated CLs were found (hence no oxygenated CL dots are present). (**c**) Re-categorized (based on the fatty acyls in *sn*-2 position) scatter plot of RSL3 induced changes in oxygenated

phospholipids. Note that AA (20:4)- and AdA (22:4)-containing phospholipid species were most responsive. (**d**) Levels of di- and tri-oxygenated PE-(C18:0/C20:4) and PE-(C18:0/C22:4) in live (cell death <15%) and ferroptotic Pfa1 cells (cell death >15%).

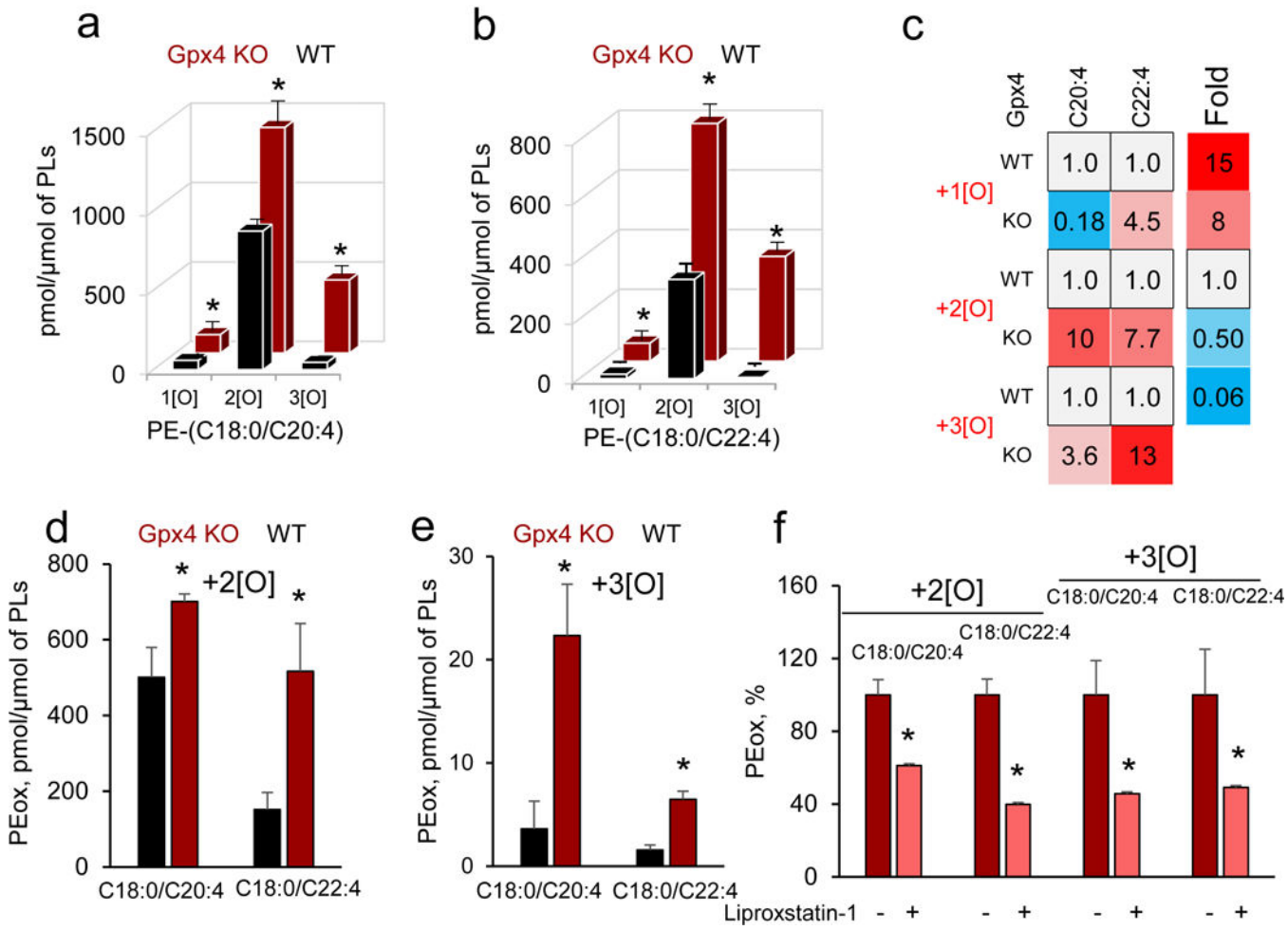

Figure 4. Oxygenated PE species are identified in ferroptotic GPX4 deficient cells and kidney of GPX4-deficient mice

(**a**) Accumulation of oxygenated PE-(C18:0/C20:4) in WT and Gpx4 KO cells. Data are mean ± s.d., n=3. **P* < 0.05 *vs.* WT Pfa1 cells (t-test). (**b**) Accumulation of oxygenated PE-(C18:0/C22:4) in WT and Gpx4 KO cells. Data are mean ± s.d., n=3. **P* < 0.05 *vs.* WT Pfa1 cells (t-test). **(c)** LC-MS based heat maps for oxygenated esterified C20:4 and C22:4 from Gpx4 WT and KO Pfa1 cells. (**d**, **e**) Elevated levels of di- and tri-oxygenated species of PE-(C18:0/C20:4) and PE-(C18:0/C22:4) in kidney of GPX4-deficient mice. Data are mean ± s.d., n=3. **P* < 0.05 *vs.* WT (t-test). (**f**) Ferroptosis inhibitor, liproxstatin-1, decreases the accumulation of di- and tri-oxygenated PE species in kidney of GPX4-deficient mice below the levels detected in WT animals. Data are mean ± s.d., n=3. **P* < 0.05 *vs.* mice without liprostatin-1 (t-test).

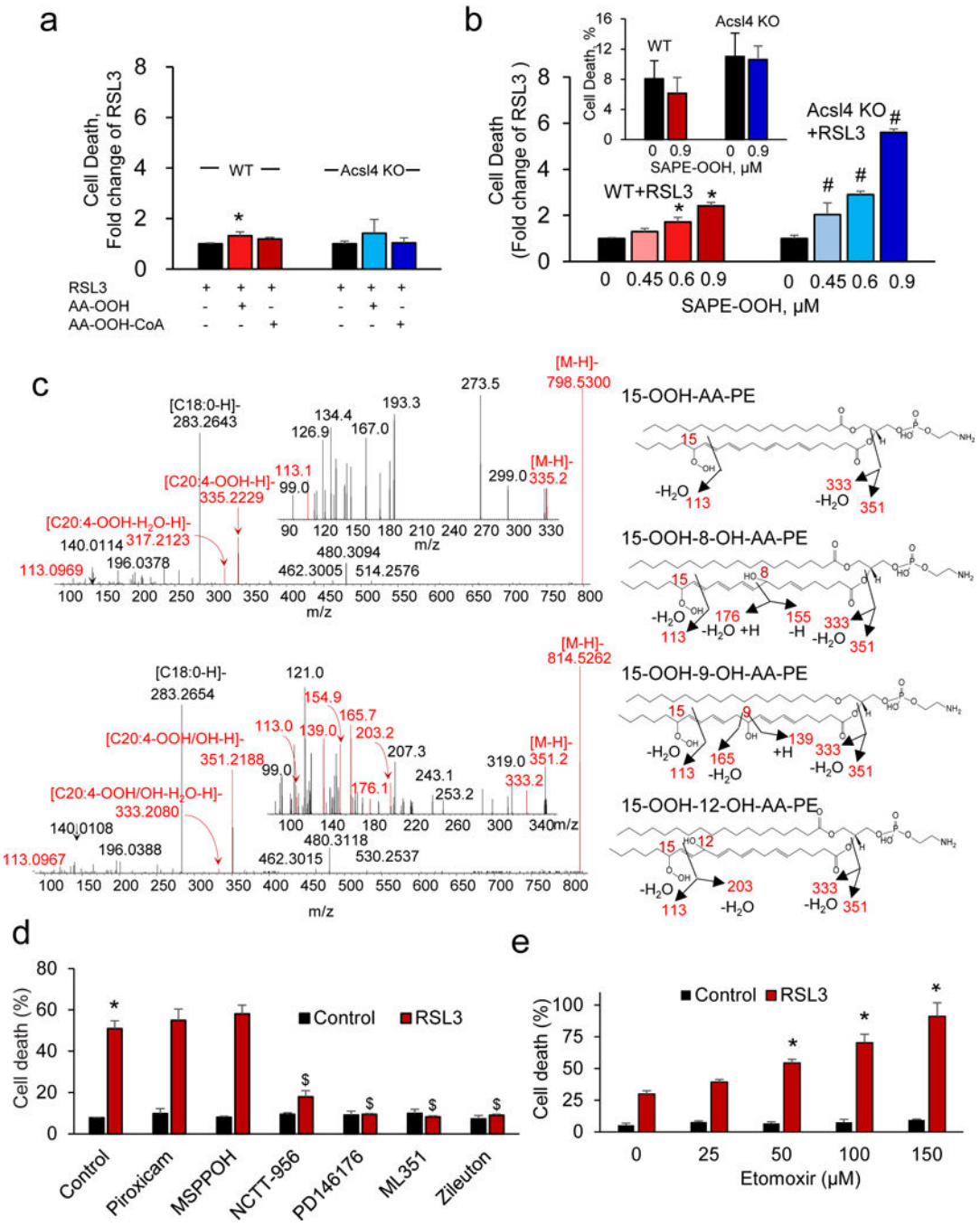

Figure 5. Labeling with *d8*-AA unravels pathways leading to oxygenated di-acylated PE ferroptotic signals

(**a, b**) Accumulation of non-deuterated and deuterated (insert) oxygenated PE-(18:0/20:4) (**a**) and PE-(18:0/22:4) (**b**) in WT and Acsl4 KO cells treated with d8-AA (16 hrs) and after that exposed to RSL3 (100 nM, 6 hrs). Data are mean ± s.d., n=3. **P* < 0.05 *vs.* WT Pfa1 cells (t-test). (**c**) Quantitative assessment of PE molecular species (C18:0/C20:4 and C18:0/d8-C20:4) (left panel) and (C18:0/22:4 and C18:0/d8-C22:4) (right panel) in WT and Acsl4 KO Pfa1 cells treated with d8-AA. Data are mean ± s.d., n=3. **P* < 0.05 *vs.* WT (t-

test). (**d**) 3D-representation of mass spectra of deuterated-PE from WT and Acsl4 KO cells treated with d8-AA. (**e**) Typical MS/MS spectrum illustrating fragmentation of non-oxygenated PE-(C18:0/C20:4) species as well as mono-, di-and tri-oxygenated species formed in RSL3 treated Pfa1 cells.

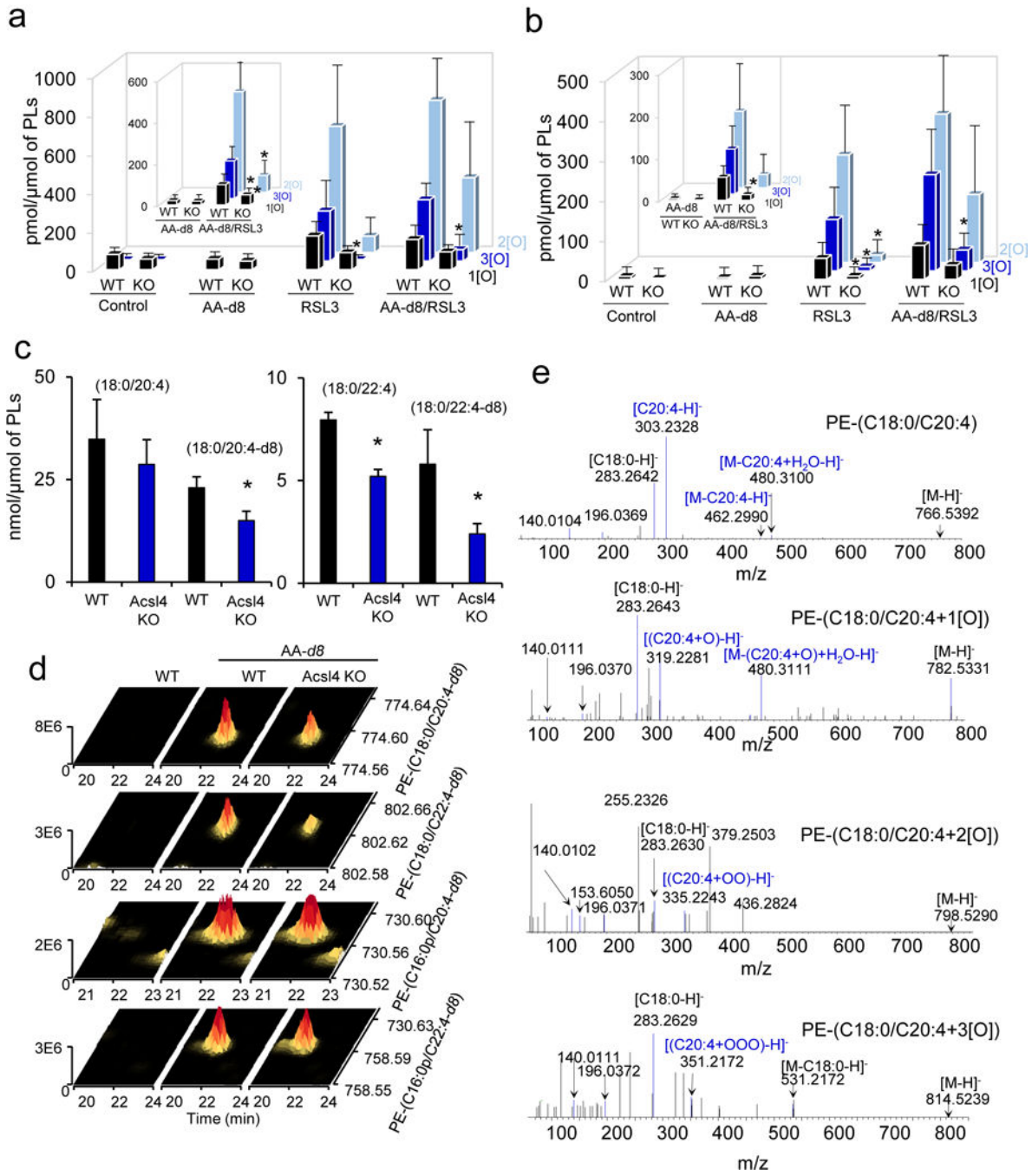

Figure 6. 15-LOX phospholipid oxidation product, 15-Hydroperoxy-SAPE, triggers ferroptosis in WT and Acsl4 KO Pfa1 cells

(**a**) Effects of AA-OOH (2.5 μM), AA-OOH-CoA (2.5 μM), and (**b**) SAPE-OOH on RSL3 (100 nM, 6 hrs) triggered ferroptosis in WT or Acsl4 KO cells. Without RSL3, SAPE-OOH (0.9 μM) did not induce ferroptosis (**b**, insert). LDH release levels: 8.1% (WT), 6.2% (WT +SAPE-OOH), 11% (Acsl4 KO), 10.6% (Acsl4 KO+SAPE-OOH). Data are mean±s.d., n=3; *,# indicate $P < 0.05$ *vs.* WT, Acsl4 KO, respectively (t-test). (**c**) LC-MS identification of 15-LOX induced SAPE oxidation products in cell lysates. Left panels: MS^2 and MS^3 (inserts)

fragmentation of di- (m/z 798.5300) and tri-oxygenated (m/z 814.5262) SAPE. Right panels: formulas of oxygenated SAPE and detected fragments (red). Identified products were: 15-OOH-AA-PE, 15-OOH-8-OH-AA-PE, 15-OOH-9-OH-AA-PE, and 15-OOH-12-OH-AA-PE. Characteristic fragments formed: m/z 351 and m/z 333 - carboxylate anions of AA-OOH and AA-OOH minus H2O, respectively; m/z 113 - OOH at 15th carbon of AA; 176 and 155, 165 and 139, 203 - OH at 8th, 9th and 12th carbons of AA. (**d**) Inhibitors of LOX (but not COX or P450) protect WT cells against RSL3 (50 nM, 18 hrs) induced ferroptosis. Inhibitors: 12/15LOX-ML351 (10 μM), 15LOX-PD146176 (0.5 μM), COX-piroxicam (20 μM), P450-MSPPOH (10 μM), 5LOX-zileuton (10 μM), 12LOX-NCTT-956 (20 μM). Data are mean±s.d., n=3. *,$ indicate $P < 0.05$ *vs.* control, RSL3, respectively (t-test). (**e**) Etomoxir (β-oxidation inhibitor) enhances RSL3 (100 nM, 6 hrs) induced ferroptosis in WT cells. Data are mean±s.d., n=3. *$P < 0.05$ *vs.* RSL3 without etomoxir (t-test).